Economic Geology

BULLETIN OF THE SOCIETY OF ECONOMIC GEOLOGISTS

VOL. 116 December No. 8

# The Teena Zn-Pb Deposit (McArthur Basin, Australia). Part I: Syndiagenetic Base Metal Sulfide Mineralization Related to Dynamic Subbasin Evolution

N. Hayward,[1,†] J. M. Magnall,[2] M. Taylor,[1] R. King,[3] N. McMillan,[4] and S. A. Gleeson[2,5]

[1]*Teck Australia Pty. Ltd., P.O. Box 1677, Western Australia 6872, Australia*

[2]*GFZ German Research Centre for Geosciences, 14473 Potsdam, Germany*

[3]*De Grey Mining Ltd., 22 Railway Road, Subiaco, Western Australia 6008, Australia*

[4]*School of Earth Sciences, University of Melbourne, Parkville, Victoria 3010, Australia*

[5]*Institute of Geological Sciences, Freie Universität Berlin, Malteserstrasse, 74-100, Berlin 12249, Germany*

## Abstract

Divergent genetic models have been proposed for clastic dominant (CD-type) massive sulfide Zn-Pb mineralization in the Proterozoic Carpentaria Zn Province. Due to varying degrees of tectonic overprint, it has been difficult to accurately constrain structural and paragenetic timing aspects of the CD-type genetic model, and the most basic timing constraints (syngenetic vs. epigenetic, synextension vs. syninversion) remain debated. The recently discovered Teena Zn-Pb deposit is hosted by an exceptionally well preserved subbasin that permits relative timing relationships to be well defined. Using a combination of geophysical, structural, sedimentological, and petrographic datasets, a new model for subbasin development and syndiagenetic hydrothermal replacement mineralization is developed for the Teena mineral system.

At Teena, sulfide mineralization was deposited from lateral fluid flow beneath an impermeable seal several hundred meters below the paleosurface and maximum flood surface, after formation of fine-grained diagenetic pyrite (py1) and dolomite nodules. Sulfide mineralization resulted from syndiagenetic carbonate replacement and pore space cementation where thermochemical sulfate reduction took place. The sulfide mineralization is therefore partly cospatial but not cogenetic with its thick pyritic hanging wall, and its lateral alteration footprint is much smaller than predicted by sedimentary exhalative (SEDEX) models. An additional zone of low-grade Zn-Pb mineralization in the footwall W-Fold Shale Member represents a different style of mineralization not previously reported for Carpentaria CD-type Zn deposits: it is associated with strata-bound lenses of hydrothermal dolomite (HTD) that formed by both replacement and carbonate dissolution and infill, which yielded diverse cavity-infill textures that include coarse-bladed dolomite fans cemented by interstitial sphalerite, dolomite, and quartz. Volumetrically minor Zn mineralization is also present in a fault conduit hydrothermal breccia and in hanging-wall synorogenic vein sets derived by hydrothermal leaching and remobilization of Zn from the underlying mineralized zones.

Whereas both the Teena and nearby McArthur River Zn-Pb deposits are located along the northern margin of the 3rd-order Hot Spring-Emu subbasin, they formed in separate 4th-order subbasins in association with local extensional growth faults. Growth fault movement in the Teena subbasin was initiated during deposition of the W-Fold Shale Member and persisted episodically until a weak structural disconformity associated with sedimentary facies regression developed in the Upper HYC unit. Shifting patterns in depocenter location, sedimentary facies development, mineralization, and alteration zonation are attributed to progressive growth and linkage of segments of a regionally anomalous ENE-trending, synsedimentary fault zone. Similar patterns of extensional subbasin development were repeated in other Zn-mineralized subbasins throughout the River supersequence across the northern Carpentaria Zn Province, and formed in response to a short-lived episode of north-northwest–south-southeast regional extension around ca 1640 ± 5 Ma, triggered by far-field subduction events.

## Introduction

A major proportion of global base metal resources are contained in sulfide minerals located in sedimentary rocks deposited in ancient marine environments (Mudd et al., 2017). The largest, highest grade deposits are hosted by siliciclastic rocks and comprise laterally extensive stratiform to strata-bound orebodies (Leach et al., 2005). The most widely applied genetic model involves sulfide precipitation following the exhalation or venting of hydrothermal fluids into sulfidic (euxinic) sea-

[†]Corresponding author: e-mail, nick.hayward@teck.com





*Submitted: February 3, 2021 / Accepted: February 7, 2021*

water and is referred to as sedimentary exhalative (SEDEX; Carne and Cathro, 1982). As many deposits lack direct evidence of exhalative processes and may preserve evidence of subseafloor replacement, there is consensus for the use of nongenetic terminology (Leach et al. 2010). A universal feature of these deposits is a close affinity with carbonaceous mudstones and siltstones, meaning shale-hosted massive sulfide (SHMS) has been a commonly used term among industry and academic geologists alike. Nevertheless, many deposits are not strictly hosted by shale, and so clastic dominant (CD-type; Leach et al. 2010) is used herein as the preferred nomenclature.

Many of the largest CD-type deposits were discovered at shallow depths (<100 m) and future discovery targets will inevitably be at deeper levels of burial with no obvious surface expression. Continued efforts to improve global discovery rates will require more predictive approaches with rigorous evaluation of the different geologic attributes that determine basin fertility and deposit location, and improvements in the technologies that permit deeper levels of detection of mineralization and alteration halos. Over the last 25 years the largest CD-type Zn discoveries have been made at depths greater than 500 m below surface and include Teena (2013, Australia; Taylor et al., 2017), Anarraaq and Aktigiruq (1999 and 2001, respectively, USA; Jennings and King, 2002; Blevings et al., 2013). Exposure to these systems has provided the authors valuable opportunities to further research models of ore genesis and exploration.

The Proterozoic Isa Superbasin, which includes the McArthur and Mt. Isa Basins (Fig. 1A), hosts several of the world's largest CD-type Zn deposits in what is also known as the Carpentaria Zn Province. The Carpentaria Zn Province is the most endowed Zn Province in the world, accounting for nearly 30% of the world's Zn resources (Huston et al., 2006). The stratigraphy of the Mt. Isa and McArthur Basins preserves a protracted record of basin evolution (1.82–1.58 Ga) in a distal continental back-arc setting (Scott et al., 2000; Giles et al., 2002). One of the longstanding debates in the Carpentaria Zn Province concerns the nature of the dominant stress regime during metallogenesis. For example, different workers have proposed that Zn mineralization may have occurred during extension (e.g., Etheridge and Wall, 1994; Neudert and McGeough, 1996) or transtension (e.g., McGoldrick et al., 2010), although more recently it has been argued that the majority of the Carpentaria Zn deposits formed during basin inversion (Gibson et al., 2017).

The geodynamic setting and associated stress regime are directly linked to a second area of debate in the Carpentaria Zn Province, which concerns the timing of mineralization relative to host sedimentation. Did hydrothermal activity occur during basin extension and involve sedimentary exhalative processes (e.g., Large et al., 1998) or early diagenetic subseafloor replacement (e.g., Williams, 1978)? Alternatively, did mineralization form by replacement processes during later basin inversion (Broadbent et al., 1998; Gibson et al., 2017)

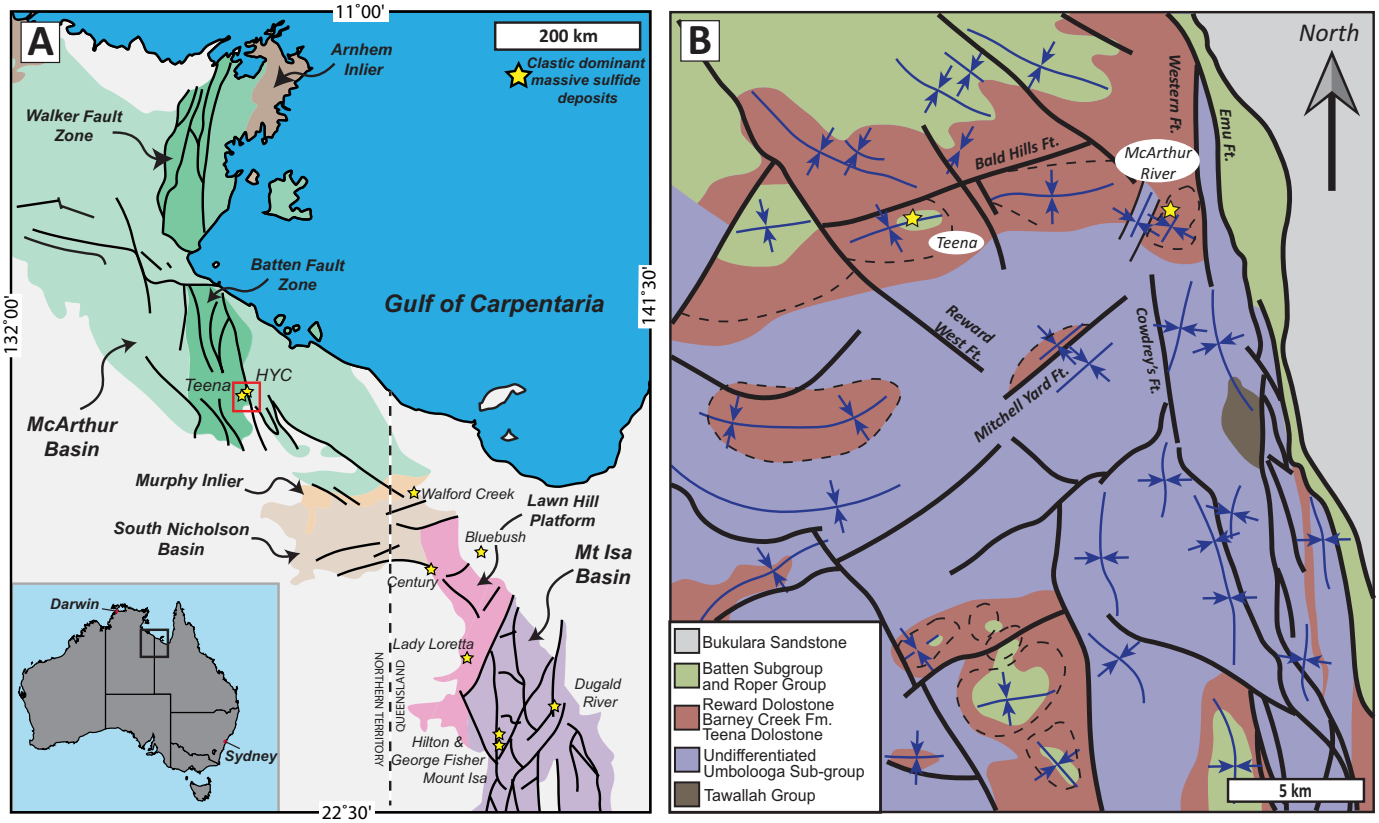


Fig. 1. A. The geographic extent of the McArthur and Mt. Isa Basins, showing major geologic terranes, fault boundaries, and CD-type deposits. The red box marks the approximate area of (B), showing a plan view interpreted geologic map of the 3rd-order Emu-Hot Springs subbasin, where CD-type deposits (yellow stars) and prospects (yellow circles) occur in smaller, fault-bound, 4th-order basins. Modified after McGoldrick et al. (2010).

under a compressional stress regime? Both the geodynamic setting and relative timing of mineralization are related and provide a fundamental basis for exploration models. For example, constraining the orientation and evolution of faults associated with hydrothermal activity is critical for identifying targets under cover. Alteration footprint models also differ markedly depending on the timing of mineralization and the diagenetic evolution of the host sequence (e.g., Magnall et al., 2021). Nevertheless, only a limited number of studies have characterized the dynamic interaction among faulting, subbasin development, sedimentation, and fluid flow at the deposit scale for CD-type mineral systems (e.g., Hinman, 1995; Broadbent et al., 1998). The paucity of studies partly corresponds with the challenges associated with interpreting primary features—whether sedimentological, diagenetic, or hydrothermal—in rocks that have frequently been affected by orogenic deformation and metamorphism; however, it also relates to the challenge of integrating different types of geologic data (e.g., structural, petrographic, geochemical) collected across different scales.

This study focusses on the Teena deposit, which has an inferred resource of 58.0 million metric tons (Mt) at 11.1% Zn and 1.6% Pb (Rox Resources, 2016). The Teena deposit is located in a subbasin 8 km west of the neighboring McArthur River (HYC) mine (Fig. 1B), which had a premine total resource of 227 Mt at 9.25% Zn, 4.1% Pb, and 41g/t Ag (Gustafson and Williams, 1981). The stratigraphy in this part of the Carpentaria Zn Province has undergone very little deformation and is essentially unmetamorphosed (Magnall et al., 2021) and, therefore, represents an ideal natural laboratory in which to interpret primary features. Notably, mineralization in the Teena subbasin occurs in two stratigraphic intervals. The first contains high-grade, fine-grained stratiform Zn-Pb sulfide mineralization in carbonaceous mudstones, which is typical of CD-type deposits. The second interval, however, is found in the underlying stratigraphic unit and comprises two styles of Zn-Pb mineralization: (1) low-grade, fine-grained stratiform sulfides and (2) coarse-grained sulfides hosted in strata-bound dolomite lenses. This latter mineralization style has not previously been described in any of the Carpentaria CD-type deposits.

This study is the first of two papers. The first paper describes and interprets the architecture of the Teena subbasin together with the major lithofacies and dominant mineralization styles (this study; Part I); the second paper describes and interprets the spatial and temporal controls on diagenetic and hydrothermal mass transfer (Part II: Magnall et al., 2021). A number of new data sets (petrographic, geochemical, geophysical), including the first published interpreted seismic section for a CD-type deposit in the McArthur Basin, have been integrated to facilitate development of a comprehensive model for subbasin evolution and the genesis of a major mineral system.

## District Geology

### *Stratigraphy*

The stratigraphy of the Mt. Isa and McArthur Basins is subdivided into three cycles of basin evolution, termed the Leichardt, Calvert, and Isa Superbasins (Jackson and Southgate, 2000; Krassay et al., 2000). These 1st-order superbasins contain a series of unconformity-bounded supersequences, which form the basis of regional chronostratigraphic correlations that each represent deposition over 10 to 20 m.y. (e.g., Southgate et al., 2000). The older Leichardt and Calvert Superbasins are dominated by synrift volcanic and coarse-clastic sedimentary sequences that have been interpreted as the source of the metals for the formation of younger CD-type deposits in the overlying Isa Superbasin (e.g., Cooke et al., 2000).

The majority of the CD-type deposits are located within stratigraphy of the lowermost Isa Superbasin (Large et al., 2005), which was predominantly associated with the thermal subsidence phase of rift development (Betts et al., 2003). In the southern McArthur Basin, CD-type mineralization is hosted by the River supersequence (Fig. 2), which has been subdivided into 3rd-order depositional cycles (Emmerugga, Barney Creek, and Lynott) that each span 1 to 5 m.y. (Jackson et al., 2000; McGoldrick et al., 2010). Much of the River supersequence in the southern McArthur Basin contains evaporite-bearing and dolomite-rich lithofacies deposited in shallow-marine to sabkha environments (Kunzmann et al., 2019). The Teena and McArthur River (HYC) deposits are hosted by the Barney Creek Formation, which represents the peak transgressive phase of the River supersequence and is bracketed by U-Pb SHRIMP detrital zircon ages for the underlying Teena Dolostone (1639 ± 6 Ma) and the overlying Lynott Formation (1636 ± 4 Ma; Page et al., 2000). Tuffaceous volcaniclastic beds in the central Barney Creek Formation yielded U-Pb SHRIMP ages of 1638 ± 7, 1639 ± 3, and 1640 ± 3 Ma (Page and Sweet, 1998).

Some of the thickest parts of the Barney Creek Formation occur in the Hot Spring-Emu subbasin (Duffett et al., 2007), which hosts the McArthur River (HYC) deposit in the northeast corner, and the Teena deposit farther west along the Bald Hills fault (Fig. 1B). The Barney Creek Formation is regionally subdivided into the lower W-Fold Shale Member, the overlying HYC Pyritic Shale Member, and the locally developed Cooley Dolostone Member (Jackson et al., 1987; Pietsch et al., 1991), each of which exhibit wedge-shaped geometries with abrupt thickening proximal to syndepositional growth faults (Fig. 2; e.g., McGoldrick et al., 2010; Kunzmann et al. 2019). The Barney Creek Formation preserves marked lateral lithofacies variations and local unconformities that indicate changes in depositional setting from a carbonate-dominated, stable, shallow-marine platform, to compartmentalized basins with numerous subbasins and local paleohighs associated with the onset of syndepositional extensional faulting and marine transgression (McGoldrick et al., 2010). There are multiple marine transgressions that can be mapped across subbasins by the preservation of pyritic and carbonaceous facies that represent maximum flooding surfaces (MFS). Two MFS have been identified in the Teena subbasin (Magnall et al., 2020), which can be correlated across other subbasins in regional studies of the Barney Creek Formation in the southern McArthur Basin (Kunzmann et al., 2019).

### *Basin architecture and structure*

Facies variations within stratigraphic sequences in the 1st-order Isa Superbasin were influenced by the hierarchy of tectonic subbasin architecture that developed at different scales.

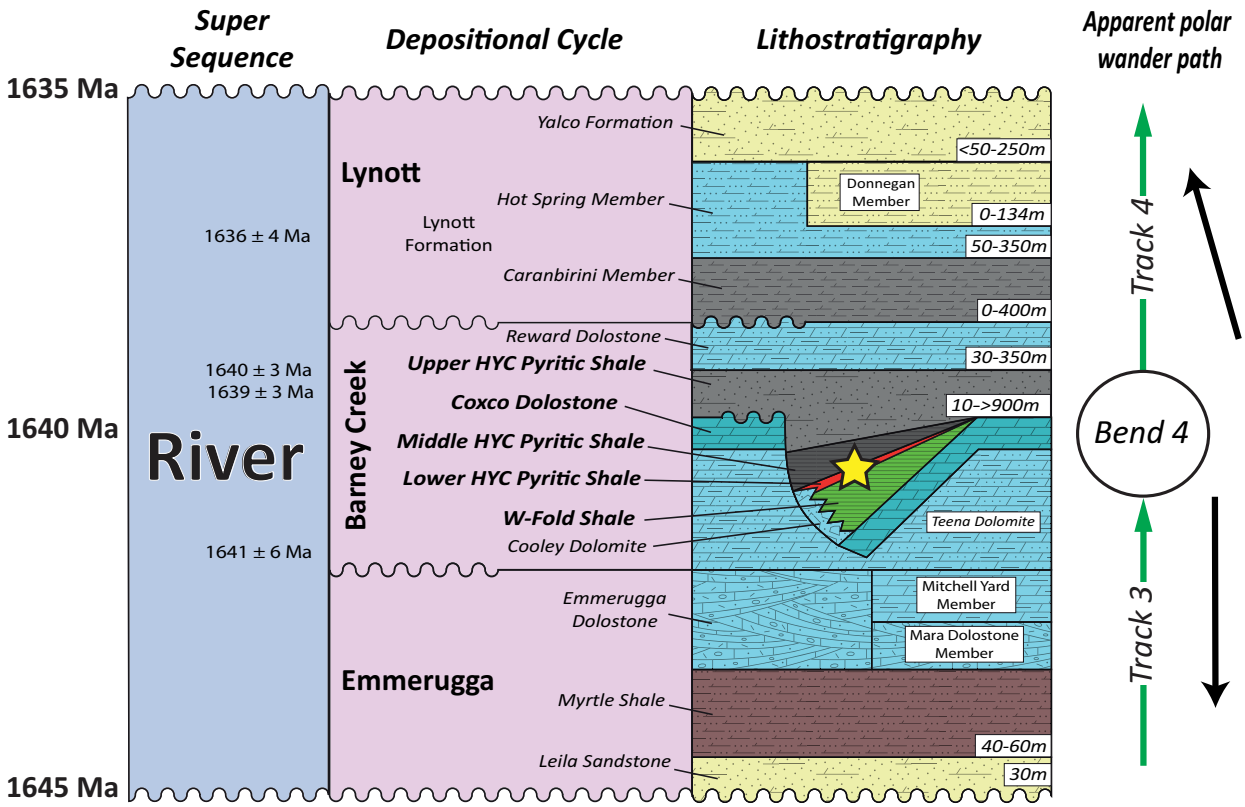


Fig. 2. A chronostratigraphic chart for the River supersequence in the Emu-Hot Springs subbasin. Approximate unit thicknesses and age constraints are compiled from Jackson et al. (1987) and Ahmad et al. (2013). The apparent polar wander path is provided by Idnurm (2000).

Within the 2nd-order ($10^3$ km$^2$) Mt. Isa and McArthur Basins there are a series of smaller fault-bound subbasins (Fig. 1B). The Teena and McArthur River deposits are located in the Batten fault zone, which is a 50- to 100-km-wide corridor of N-trending faults that bounds the 3rd-order ($10^2$ km$^2$) Hot Spring-Emu subbasin.

Regional fault offsets in the Batten fault zone resulted in stratigraphy of the Paleoproterozoic McArthur Group being exposed between younger Mesoproterozoic to Cambrian cover sequence packages to the west and east (Fig. 1). The eastern margin of the Batten fault zone is bound by the syn-rift Emu fault zone and the western margin is bound by the synorogenic, E-verging Tawallah-Abner and Scrutton thrust faults (Rawlings et al., 2004). An easterly-trending horst (Urapunga fault zone) separates the Batten from the Walker fault zone, which has similar orientation, size, and evolution to the Batten fault zone. Internally, the Batten fault zone is compartmentalized by a series of WNW-, ENE-, and NNW-trending fault sets. On the east side of the Batten fault zone, most large-scale folds are oriented roughly north-northwest, subparallel to the Emu fault, whereas farther west in the Hot Spring-Emu subbasin, small synclinal subbasins and medium-scale folds trend east-northeast, subparallel to ENE- trending faults (Fig. 1B; Pietsch et al., 1991; McGoldrick et al., 2010). Within the Hot Spring-Emu subbasin, several smaller 4th-order ($10^1$ km$^2$) subbasins are associated with the thickest accumulations of Barney Creek Formation in paleodepocenters, some of which host CD-type mineralization (Fig. 1B).

*Geodynamic setting and tectonic models*

From the late 1990s there was broad agreement that the stratigraphy hosting the Carpentaria Zn deposits was deposited in a far-field back-arc setting linked to collision and subduction along the southern margin of the North Australian craton (NAC; Scott et al., 2000; Betts et al., 2002, 2006). More recently, however, Betts et al. (2016) argued that the Calvert and Isa Superbasins were deposited inboard of a passive margin to an internal ocean between the east margin of the North Australian craton and Laurentia. W-dipping subduction beneath the North Australian craton subsequently resulted in the closure of this ocean basin around 1640 Ma (coincident with the River supersequence) and culminated in the collisional Isan orogeny between 1600 and 1500 Ma. Gibson et al. (2017) proposed that ocean closure and synorogenic inversion may have commenced earlier, between 1650 to 1640 Ma, before a renewed period of northeast-southwest extension between 1640 to 1620 Ma resulted in the deposition of the River supersequence.

The formation of CD-type deposits in the River supersequence around ca. 1640 Ma coincided with a major inflection in the Apparent Polar Wandering Path (Fig. 2; Idnurm, 2000). Tectonism associated with this plate reorganization event has been widely attributed as a trigger for Zn metallogenesis in the Mt. Isa and McArthur Basins at 1640 Ma, although specific details are disputed. Historically, most authors favored an extensional rift to transtensional pull-apart setting linked to either NNW-SSE extension (e.g., Plumb and Wellman, 1987), north-

south extension (Etheridge and Wall, 1994; Neudert and McGeough, 1996; McGoldrick et al., 2010), or NNE-SSW extension (Betts et al., 2016). Hinman (1995) and Rogers (1996) proposed that an episode of northwest-southeast compression caused local inversion and sinistral transpression along the Emu fault during the late stages of Barney Creek Formation deposition. Contrary to the widely accepted synextension models for deposit formation, Gibson et al (2017) recently proposed that most CD-type deposits in the Mount Isa region formed syninversion with NE-SW-directed crustal shortening during the 1650 to 1640 Ma Riversleigh Inversion Event, or in the case of the Century Zn deposit (ca. 1585 Ma; Broadbent et al., 1998), during onset of the regional Isan orogeny.

The main phase of the Isan orogeny occurred between 1600 to 1500 Ma in association with collisional events along the eastern margin of the North Australian craton (e.g., Giles et al., 2006). The effects of the Isan orogeny deformation and metamorphism are most intensely developed in the southeast portion of the Isa inlier, where upper amphibolite facies rocks are exposed. Regional $D_1$ fold and thrusts resulted from north-south to NNW-SSE thin-skinned shortening and basin inversion around 1600 to 1575 Ma. This event was followed by peak metamorphism with generally east-west $D_2$ shortening between 1570 to 1550 Ma. Between 1550 to 1530 Ma the Isan orogeny switched to $D_3$-$D_4$ oblique transpressional phases dominated by NW-trending sinistral wrench faults and later NE-trending dextral faults. In southeastern parts of the province this deformation also coincided with synorogenic granite emplacement. The metamorphic grade generally decreases toward the northwest to subgreenschist facies in the McArthur Basin. Much of the River supersequence in the Teena subbasin only underwent weak deformation and very low-grade metamorphism (Magnall et al., 2021).

## Discovery History

The Teena deposit was discovered in 2013 by Teck Australia Pty. Ltd. (Teck) in partnership with Rox Resources Ltd. Discovery followed a process of systematic targeting of underexplored prospective subbasins, which were interpreted to have been bound by the growth faults that developed during the Barney Creek deposition cycle. Priority was given to subbasins developed along the E-trending Bald Hills fault, based on company conceptual exploration models and historic open-file company reports that established evidence for district-scale Zn-Pb mineralization and syndepositional extensional faulting along this fault zone.

Initial exploration of the subbasin included reinterpretation of historic helimagnetic data to define the extent of the subbasin, together with a new airborne gravity gradiometer survey that yielded a higher amplitude response over the interpreted subbasin than could be accounted for by typical lithostratigraphy alone and was considered permissive of thick sulfide accumulation. A subsequent review of historic drill core data from three diamond holes, drilled in the mid-1970s by Mount Isa Mines Limited on the margins of the subbasin, confirmed the presence of the mineralized Lower HYC Pyritic Shale Member of the Barney Creek Formation (Fig. 2), including an interval of 9.2 m at 3.5% Zn. A further five diamond drill holes were identified, previously unreported in historical data compilations, which revealed that the HYC Pyritic Shale Member thickened toward the northern margin of the subbasin. The thickest intercepts comprised thin, low-grade intervals of fine-grained stratiform sphalerite as well as medium-grained disseminated sphalerite and galena replacement of dolostone lenses in the Barney Creek Formation.

The evidence of stratiform Zn mineralization, together with recognition that the interpreted depocenter of the subbasin had not yet been drilled, led to a preliminary 4-hole diamond drill program in July 2013. The initial drill test returned high-grade Zn and Pb mineralization in multiple horizons in all holes along the synclinal axis of the basin, including 16.2 m grading 17.2% Zn + Pb from 1,070.3 m (Rox Resources, 2013).

## Methods

### *Geology field mapping and drilling*

Integrated two- and three-dimensional geologic models for the Teena deposit and subbasin are constrained in this study by historic 1:5000-scale outcrop geology and structure mapping, as well as drill core from 33 diamond drill holes, several of which extend to >1,000 m deep. Drill core for all Teck drill holes was routinely oriented and logged for lithology, stratigraphy, structure, and alteration. Oriented drill core for all diamond drill holes was routinely structurally logged, using either alpha/beta measurements or a Reflex IQ-Logger tool. High-resolution photography (wet and dry) of all drill core was carried out and characteristic samples of each unit were selected for further evaluation using standard petrographic techniques (binocular microscope, transmitted and reflected light microscopy). Detailed stratigraphic logging correlations are supported with natural gamma logs for most drill holes. Alteration mapping was supplemented by CoreScan hyperspectral (visible near- and short wave-infrared) logging of core from two holes (TNDD015, TNDD022), as well as spot short wave-infrared analyses on core using a TerraSpec® instrument. Mineralized core was routinely sampled in 30- to 100-cm intervals and assayed for multiple elements by a range of element-specific techniques, including fused bead laser ablation ICP-MS and mass spectrometer quantitative analysis using acid-free digestion, by either Bureau Veritas (Mt. Isa), Ultratrace (Perth), or ACME (Vancouver) laboratories.

### *Geophysics*

Project- and district-scale mapping are supported with analysis of a detailed helimagmatic survey, acquisition of an airborne Falcon gravity survey, as well as local magnetotelluric and ground electromagnetic grid surveys. A single 12-km-long Vibroseis seismic reflection traverse (Line 2015-01) across the deposit was also acquired using a 10- to 140-Hz frequency sweep. Geophones were placed with a nominal offset of 5,000 m providing a fold of 1,000. Seismic processing by Velseis Processing Pty. Ltd. used a standard Pre-Stack Time Migration processing sequence.

Wireline logging was performed on all new diamond drill holes to define the petrophysical signature of the different stratigraphic units. Natural gamma, magnetic susceptibility, density, and inductive conductivity were measured and compared with observed lithologic and geochemical changes in different stratigraphic units.

*Basin restoration and sediment decompaction*

In order to model the primary Teena subbasin architecture and depositional environment, the true thickness and horizontal length of each sedimentary unit was determined from manual flexural-slip unfolding of serial sections derived from the three-dimensional Leapfrog model. Maximum primary depositional thicknesses were determined using the 1st-order approximation method described by Angevine et al. (1990). In this method, the progressive decrease in porosity that occurs with increasing burial depth, from 0 to 7 km, is quantified for a range of primary sedimentary rocks types.

## Results

*Lithostratigraphy*

*Teena Dolostone*: The Teena Dolostone is the oldest stratigraphic formation in the Teena deposit area and only partially intersected by drilling. Drill intercepts indicate that it is thicker (>100 m) than typically observed elsewhere in Hot Spring-Emu subbasin (<60 m; Ahmad et al., 2013). The Teena Dolostone in the Teena subbasin typically comprises fine-grained to micritic light-gray recrystallized dolostone. Where primary bedding textures are preserved, planar laminated silty dolostones and dolomitic sandstones predominate, with minor slump and rare algal lamination textures. The upper contact with the overlying W-Fold Shale Member of the Barney Creek Formation is generally gradational; however, sharp erosional contacts are locally developed in the footwall of the Bald Hills fault zone and interpreted to represent locally emergent conditions. The Coxco Dolostone Member of the upper Teena Dolostone is not encountered in any of the drill intercepts in the Teena subbasin, although it has been mapped elsewhere in the Hot Spring-Emu subbasin. This member represents a local facies distinguished by the presence of distinctive upward-radiating fans of acicular dolomite crystals ("Coxco Needles;" Pietsch et al., 1991), formed by replacement of either seafloor aragonite or gypsum crystals (Ahmad et al., 2013, and references therein).

*W-Fold Shale Member*: Regionally, the W-Fold Shale Member is characterized by distinctive, thin-bedded, green and red dolomitic siltstone and shale. Within the Teena subbasin, the W-Fold Shale Member is anomalously thick (up to 300 m) and has highly variable vertical and lateral lithofacies that become overall finer grained upsection and thin toward the south. Despite its stratigraphic name, this member contains only a minor proportion of shale. The lower portion transitions from thinly interbedded sandy dolostone, to thin-bedded graded cycles of fine-grained dolomitic arkosic sandstone and green dolomitic siltstone with abundant pale gray to reddish, nodular dolostone beds. The middle portion is generally finer gained with interbedded sequences (1–5 m thick) of dark gray to dark green, carbonaceous, chloritic, and weakly pyritic laminated siltstone and fine sandstone, as well as subordinate dolomite cemented, fine-grained, sandstone beds. Pyritic and carbonaceous mudstone beds locally contain centimeter-scale ovoid dolomite nodules in the eastern portion of the Teena subbasin. The upper portion of the W-Fold Shale Member is dominated by thin-bedded to laminated, dark green siltstones and fine-grained dolomitic sandstones with abundant irregular bed-parallel dolomite nodules. It also contains several distinct graded units of poorly sorted, feldspar-rich, sandstone beds up to 10 m thick with subordinate siltstone and green claystone beds. Detrital K-feldspar in these beds appears to be of volcanic origin (Magnall et al., 2021) and these units are logged as volcaniclastic sandstone. The basal sandstone beds frequently contain carbonaceous mud chips which, together with local basal scours and cyclic normal grading, is interpreted to indicate deposition by mass-flow turbidity currents. Sedimentary textures developed throughout fine-grained siliciclastic beds in the W-Fold Shale Member include ubiquitous graded bedding, diverse dolomite nodule morphologies, flame structures, and widespread intraformational slump folds.

*HYC Pyritic Shale Member:* The HYC Pyritic Shale Member hosts the most significant mineralization in the Teena subbasin and throughout the Hot Spring-Emu subbasin. It has highly variable thickness (0–650 m) in the Teena subbasin and has been informally subdivided by Teck geologists into three distinct but completely gradational units: (1) the lower mineralized dolomitic shale unit (Lower HYC unit), (2) the middle pyritic shale unit (Middle HYC unit), and (3) an upper carbonaceous siltstone unit (Upper HYC unit). The Lower HYC unit is broadly wedge shaped, thickening toward the northeast corner of the subbasin (up to 250 m in TNDD019) and pinching out completely along the southern and western margins. It comprises facies that are generally transitional with the underlying W-Fold Shale Member, including very thin-bedded to laminated dolomitic, pyritic and carbonaceous siltstones and mudstones, which become progressively less dolomitic and more pyritic (up to 80%) upsequence. This unit also hosts the two main lenses of stratiform Zn-Pb mineralization, which are separated by a volcaniclastic sandstone unit that ranges from <1 m thick along the southern subbasin margin (where the mineralized lenses merge), to 40 m thick in the easternmost section of the synclinal axis. The volcaniclastic sandstone unit comprises several graded cycles of mud-chip arkosic sandstones, siltstones, and carbonaceous mudstones. The Lower HYC unit has abundant dolomite nodules with diverse morphologies, including thin lenticular bedform nodules, small (<8 mm) spherical nodules with radiaxial fibers, and large (up to 10 cm) ovoid nodules. The larger dolomite nodules typically preserve inclusion trails of replaced bedding laminae and show compaction-related warping of adjacent sedimentary layering. Partly compacted, worm-like dolomite veinlets and irregular dolomite nodules are also found in the volcaniclastic sandstone beds. The top of the Lower HYC unit is locally defined by the upper limit of large ovoid dolomite nodules in black carbonaceous siltstone. The bottom contact with the W-Fold Shale Member is informally defined by a volcaniclastic sandstone marker bed, located near the gradation from predominantly chloritic dolomitic siltstones to predominantly carbonaceous dolomitic siltstones. Rare, thin sedimentary breccia beds (10–30 cm), comprising matrix-supported, subangular to subrounded, dolostone clasts, are observed in drill holes located immediately adjacent to extensional faults along the northern margin of the subbasin, and do not appear to persist laterally for more than several 10s m.

The Middle HYC unit is 50 to 350 m thick and defined by thin-bedded to massive, dark gray to black, pyritic carbonaceous siltstones and mudstones. Abundant (5–50%) very fine grained, disseminated pyrite occurs in laminated beds

throughout this interval. Dolomite nodules are rare to absent. North and south of the Teena subbasin the overall thickness and abundance of pyrite decreases dramatically in lateral equivalents to the Middle HYC unit. For example, drill hole TNDD018 located ~1.3 km south of the TNDD019 pierce point (Fig 3A) intersected only a 40-m-thick pyritic interval. The Upper HYC unit comprises 50 to 100 m of laminated to thick-bedded carbonaceous siltstone with pyrite decreasing (<25%) upsequence, interbedded with upward increasing fine-grained sandstone, sandy dolostone, and dolomitic siltstone. The uppermost Barney Creek Formation is not pyritic.

*Reward Dolostone Formation:* The Reward Dolostone Formation in the Teena subbasin ranges from 300 to 350 m thick and has a gradational and conformable contact with the underlying Barney Creek Formation. It comprises predominantly thick-bedded dololutite and dolarenite, with intervals of dolomitic carbonaceous siltstones near the base, and clast-supported polymict sedimentary breccias in the middle. Dolomite nodules are common in dolomitic siltstone beds, whereas some dolostone beds in outcrop contain evaporite casts (quartz) after bladed gypsum.

*Lynott Formation:* The Lynott Formation is up to 650 m thick in the Hot Spring-Emu subbasin and subdivided into three members: the Caranbirini, Hot Springs, and Donnegan Members (Fig. 2; Jackson et al., 1987). At Teena, the Lynott Formation is poorly preserved with <50 m of the Caranbirini and Hot Spring Members exposed at the Teena Hill in the central portion of the deposit area (Fig. 3). The lower Caranbirini Member has a regionally unconformable or disconformable contact with the underlying Reward Dolomite (Jackson et al., 1987), although in the Teena subbasin the contact appears locally conformable and gradational with increasing carbonaceous mudstone content from the lower dolostone unit. This member comprises thin-bedded to laminated dolomitic siltstone and mudstone, in part moderately carbonaceous and pyritic, interbedded with silty dolomitic mudstone and fine-grained dolarenite. Minor lenses of slump breccia, ripple marks, and evaporite casts are locally present. The overlying Hot Spring Member comprises thick-bedded, fine- to medium-grained, dolomitic sandstone exhibiting ripple and hummocky cross stratification, casts of abundant halite hoppers, and gypsum rosettes.

### *Subbasin architecture and deformation*

The Teena subbasin comprises a gently folded, E-W-striking syncline in the hanging wall of the S-dipping Bald Hills fault zone (BHFZ; Fig. 1B). The subbasin has a strike length of ~5 km between two major NW-trending faults, the Reward West fault to the west and Wickens fault to the east. The Reward West fault is interpreted to be a W-dipping normal fault that separates the Teena subbasin from another similar-sized subbasin (Boko) farther west. The Wickens Hill fault, located east of Teena (Fig. 1B), is a more complicated fault corridor that comprises multiple subparallel faults bounding a narrow NW-trending horst between the Teena subbasin and another subbasin (W-Fold) located farther east. The Teena syncline is traversed by minor ENE-trending faults on the southern limb, and crosscut by two sets of minor normal faults, trending NNW (spaced ~400–500 m apart) and NNE (spaced ~1 km apart; Fig. 3A).

The Bald Hills fault zone has an easterly strike of at least 25 km, but it is not evident in published Northern Territory Geological Survey 1:100,000-scale geology maps because it has a very subtle surface expression showing little stratigraphic throw (<10 m). It is also largely recessive except for rare small outcrops of silicified fault breccia. Mapping and sparse stratigraphic drilling in the block north of the Bald Hills fault zone near Teena indicate that the footwall area has only a thin (<50 m) sequence of Barney Creek Formation, which was deposited unconformably on uplifted Teena Dolostone and Emmerugga Dolostone in a karstic platform.

In 2015 Teck ran a 12-km-long two-dimensional seismic reflection survey across the Teena subbasin and Bald Hills fault zone to better constrain the three-dimensional architecture of the subbasin, faults, and mineralization (Fig. 4). The survey did not reliably show detailed reflector geometries in the core of the plunging Teena syncline due to complications from off-section plunging reflectors. However, it did confirm historic interpretations that the Bald Hills fault zone is a major S-dipping normal fault that separates two large blocks tilted 10°-20° down to the north and revealed that it includes a prominent hanging-wall fault splay, herein named the Jabiru fault. The strike of the Jabiru fault, along with another subordinate ENE-trending fault (Kookaburra fault), is also interpreted from mapping with detailed helimagnetic and airborne gravity surveys, and locally verified by drilled fault intersections (Fig. 3B).

Where intersected by drilling in the dolomite-rich W-Fold Shale Member and Teena Dolostone, the Kookaburra and Jabiru faults have a brittle character comprising 2- to 10-m thick, monomict, mosaic to chaotic breccias with a rock flour matrix, enveloped by broad damage zones with dolomite crackle veins. However, where these faults intersect overlying carbonaceous siltstones and mudstones of the HYC Pyritic Shale Member, they have a brittle-ductile style with narrow (0.2–2 m) shears cored by matrix-supported chaotic breccia or carbonaceous clay gouge and are locally associated with meter-scale drag folds of adjacent sedimentary layering.

All significant mapped and drilled faults in the Teena subbasin are steeply dipping and have apparent bulk normal displacements ranging from 1 to 200 m, reaching a maximum drill-indicated throw of ~450 m on the Jabiru fault at the eastern portion of the study area (Fig. 3B). Displacement on the ENE-trending faults diminishes abruptly updip to <1 m in the Upper HYC unit, consistent with a synsedimentary growth origin. There is local mesoscopic evidence for minor inversion of the Jabiru and Bald Hills faults (drag folds, reverse fault kinematic indicators), but bulk reverse throw remains much less than earlier normal throw. Evidence for contractional deformation and inversion is widely expressed as frequent narrow (<20 cm) clay-rich shear zones developed along certain inclined bedding planes, where vein offsets indicate late-stage, reverse, flexural-slip displacement on the scale of centimeters, possibly up to a few meters.

In outcrop the Teena syncline is a doubly plunging syncline with approximately symmetrical limbs that dip <20° toward a very shallow-plunging axis striking ~075° (Fig. 3A). Lower down in the stratigraphic sequence structural data from oriented core logging record a different synclinal geometry (Figs. 3B, 5A). In the lower Barney Creek Formation and Teena

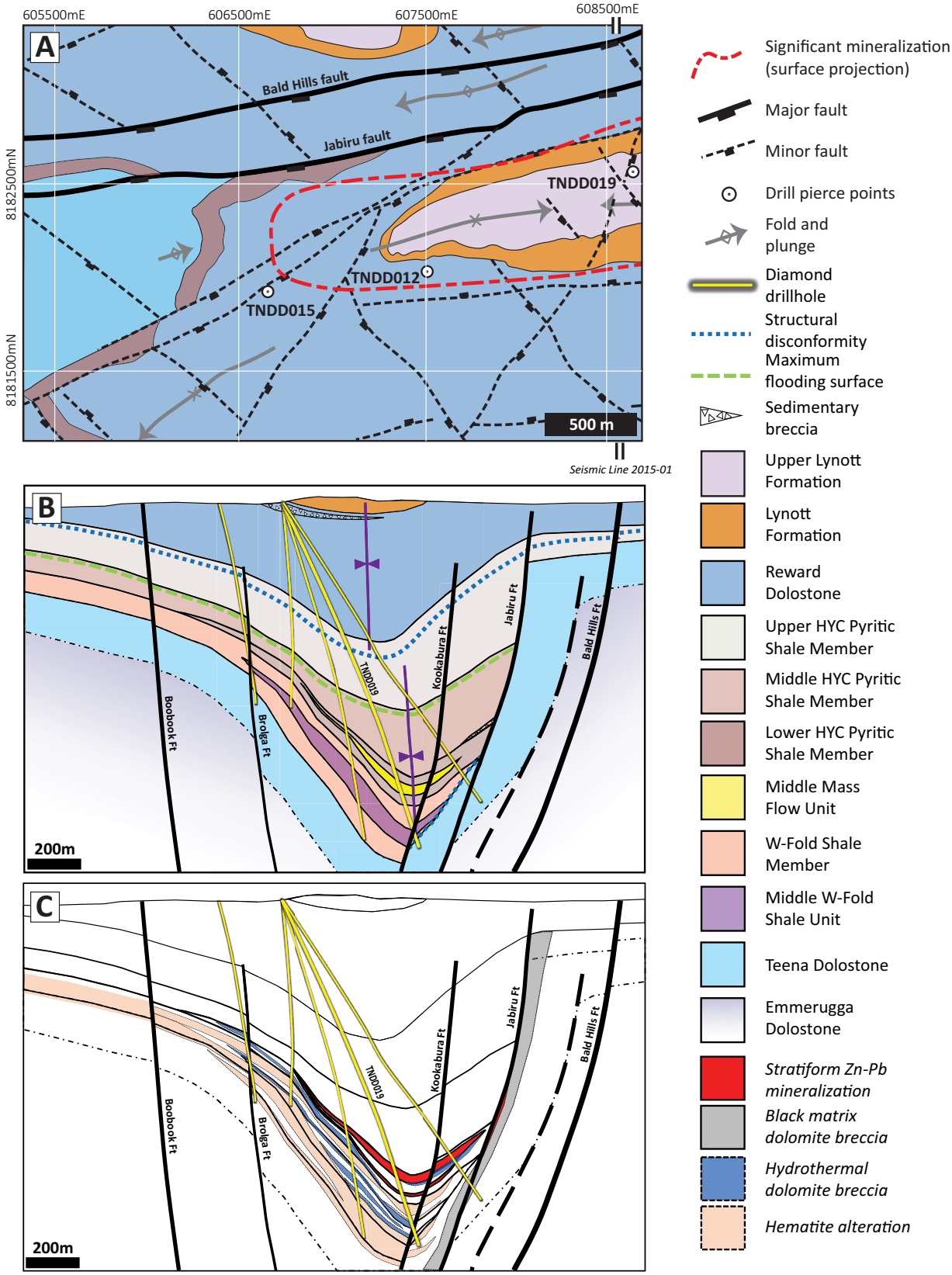


Fig. 3. A. Interpreted bedrock geologic map of the Teena subbasin on which geologic structures, drill hole collars, and the projected outline of significant Zn + Pb mineralization are shown (GDA1994 MGA-Z53 coordinates). B. Cross section 608600 mE showing stratigraphy, mineralization, and structure. C. Cross section 608600 mE showing hematite and hydrothermal dolomite (HTD) alteration.

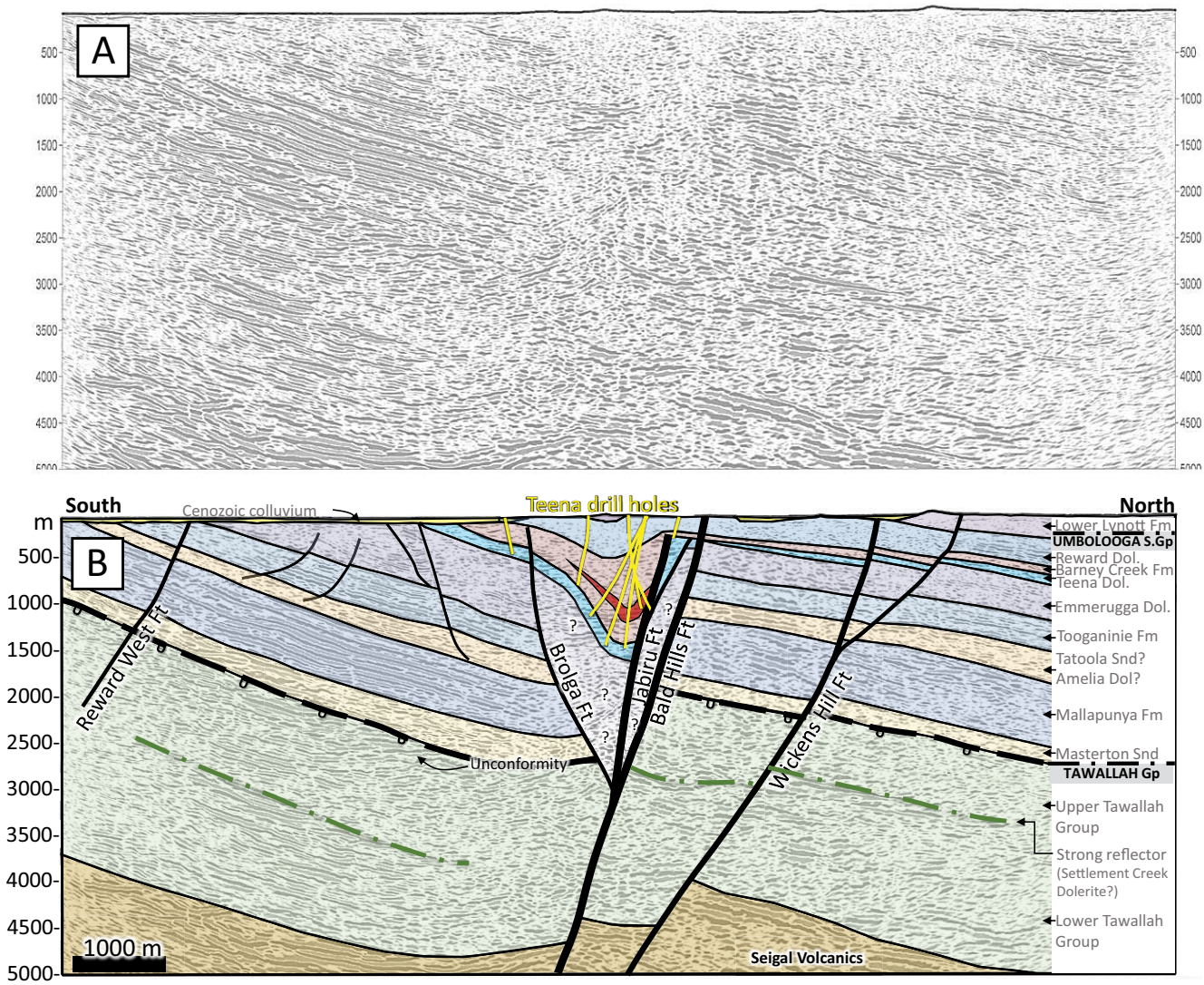


Fig. 4. Seismic reflection survey Line 2015-01 at 608400 mE (location shown in Fig. 1B). A. Grayscale reflection image of a prestack time migrated (PSTM) section converted from time to depth (m) using smoothed DMO stacking velocities that ranged from 2,200 to 6,300 m/s with increasing depth. B. Interpreted geology overlain in PSTM section. The mineralized Lower HYC unit in the Teena syncline is drill-constrained but poor-quality reflection data below the limit of drilling preclude further interpretation in the central portion. Stratigraphic abbreviations: Dol = Dolostone, Fm = Formation, S. Gp = Subgroup, Snd = Sandstone.

Dolostone, the Teena syncline is tighter and more asymmetric with a long southern limb dipping 30°-40° NNW and a short northern limb dipping 10°-40° SSE, converging about an axis that plunges 10° toward 065°. The deeper portion of the fold axis is thus more steeply plunging and rotated anticlockwise by about 10° from the shallower portion of the fold axis (Fig. 5A). Evidence of a very subtle structural discontinuity zone between the two-fold profiles occurs near the top of the HYC Pyritic Shale Member, where bedding dips shallow over several meters (Fig. 3B). The structural discontinuity zone coincides with a regressive transition in depositional facies from carbonaceous mudstones to dolomitic siltstones.

Whereas the Bald Hills fault zone bounds a simple half-graben geometry at the district scale (Fig. 4), the local geometry of the Teena subbasin in relationship to the Jabiru fault is more complicated. In the immediate hanging wall of the Jabiru fault, bedding contacts dip moderately south and define the northern limb of the Teena syncline. Along this northern limb, drill-intersected contacts between the W-Fold Shale Member and Teena Dolostone are either locally disconformable or show a slight angular unconformity (e.g., onlap unconformity). In the immediate footwall of the Jabiru fault, Teena Dolostone bedding dips moderately to steeply south, which is in marked contrast to the uniformly shallow north dips in the footwall of the Bald Hills fault zone. Consequently, it appears that all or part of the fault block between the Jabiru and Bald Hills faults is rotated to an anomalous S-downdip along the north limb of the Teena syncline. A second speculative fault may separate S- and N-dipping structural domains within this fault block (Fig. 3B), although the architecture remains highly uncertain with lack of outcrop or drill exposure.

Several meso- to microscale intraformational structural styles are observed in the Teena subbasin. Bedding-parallel stylolites and stylolaminae are common in most lithologies

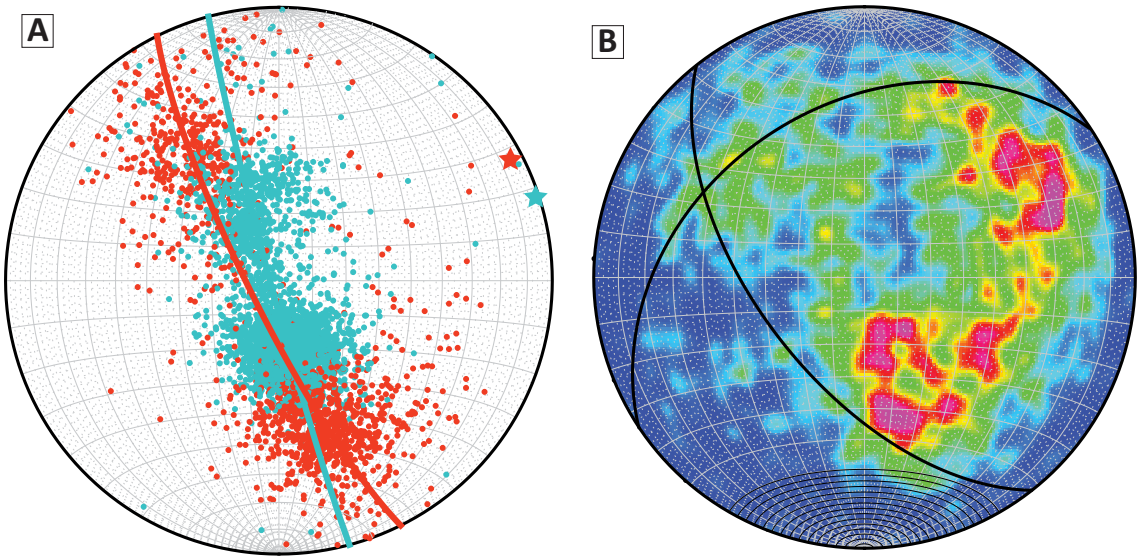


Fig. 5. Lower hemisphere equal area stereonets of structural data from Teena-oriented drill core logging. A. Poles to bedding with interpreted fold axes. The turquoise circles represent samples from the Reward Formation and orange circles are samples from the Teena Dolomite, W-Fold Shale Member, and Lower HYC unit. B. Contoured poles to all late-stage veins with interpreted mean dips.

of the Barney Creek Formation, particularly in the W-Fold Shale Member. Small-scale folds (0.1–1 m) are observed in drill core in the W-Fold Shale Member, and to a lesser extent also in the Lower HYC unit. These folds are mostly intraformational with irregular recumbent axial planes, typical of soft-sediment slump folds, and commonly show dominant N-vergence. Small-scale (cm) extensional fault sets associated with domino-style block rotation locally occur in thin dolostone interbeds in the Lower HYC unit, and rare intraformational imbricate microthrust stacks disrupt bedding contacts. Although the kinematics of these small-scale structures has not been comprehensively studied, preliminary observations from oriented drill core indicate that N-vergence dominates.

Structural core logging shows that there is a widespread but volumetrically minor generation of late-stage quartz-carbonate-sulfide veins with three sets of preferred orientations; one minor set is parallel to bedding, and the other two-dominant vein sets crosscut bedding at a high angle and dip moderately southwest (mean dip direction ~58° toward 235°) and moderately north-northwest (~35° toward 325°; Fig. 5B). Although the bed-parallel veins frequently occur in flexural slip shears, their lack of internal deformation attests to a relatively late timing. The latter two sets have a mean dihedral angle of ~60° and could have formed as conjugates, but the NW-trending vein set could also be related to crosscutting faults with similar trend (Fig. 3A). The inclined vein sets at Teena frequently all exhibit small-scale (<10 cm) reverse throw with similar style and mineralogy, suggesting they have similar timing.

### *Subbasin depocenter mapping*

Isopach maps were compiled from core logging for each member of the Barney Creek Formation in the Teena subbasin to constrain the influence of extensional fault growth on subbasin architecture and sedimentation stratigraphic thickness (Fig. 6). Isopach map construction involved flexural-slip unfolding and restoration of preserved line-lengths for each unit to a horizontal surface, section by section, to map spatial variations in true stratigraphic width and thickness. As noted above, the W-Fold Shale and HYC Pyritic Shale Members have the most variable present-day thickness. Both units are absent in footwall blocks immediately north of the Jabiru and Bald Hills faults, where nonpyritic Barney Creek Formation is deposited unconformably on Teena Dolostone. The thickest portion of the W-Fold Shale Member, interpreted to represent the original depocenter, lies central to and roughly coincident with the axis of the Teena syncline at ~607500mE. In contrast, the thickest accumulation of HYC Pyritic Shale Member occurs at least 1 km farther east, closer to the Jabiru fault, near the east edge of the study area. The thickest portion of the middle to upper Pyritic Shale Member is located near the eastern margin of the study area in the axis of the Teena syncline, whereas the lowermost parts of the overlying Reward Dolostone preserve no apparent thickness variations across the Teena syncline.

### *Mineralization styles and sulfide paragenesis*

The distribution of fine-grained pyrite in the Lower and Middle HYC units is highly variable. There are two generations of early-stage pyrite (py1a and py1b) that predate hydrothermal mineralization, and which therefore provide an important reference for determining the relative timing of hydrothermal activity in the Lower HYC unit (Magnall et al., 2020): (1) py1a comprises very fine grained (5–10 $\mu$m), disseminated, euhedral to subhedral crystals with minor framboids, as well as wispy aggregates that are parallel to sedimentary layering (Figs. 7, 8A); (2) py1b comprises coarser grained (>10 $\mu$m) idiomorphic crystals, either disseminated in mudstone laminations or on the margins of dolomite nodules (Fig. 8B). In the more dolomitic sequences of the Lower HYC unit, dolomite nodules frequently preserve internal planar inclusion trails of py1a that they overgrew,

whereas adjacent external py1 laminae are thinner and partially wrap or deflect around the nodules (Fig. 8A). There is some degree of spatial overlap of py1 with the stratiform Zn-Pb mineralization (Fig. 7), although py1 also extends up to 350 m into the hanging wall above mineralization. Later generations of pyrite (py2-py4) that are associated with mineralization are described below.

Zinc-lead sulfide mineralization at the Teena deposit occurs in both the Lower HYC unit and W-Fold Shale Member. The highest grade mineralization comprises fine-grained stratiform sphalerite beds with minor galena (e.g., Fig. 7A, B) at the top of this mineralized sequence, in the Lower HYC unit, where it forms two massive sulfide lenses (Main and Lower lenses; Fig. 3). A third lower grade interval of Zn-Pb mineralization (Footwall lens) occurs in the middle W-Fold Shale Member. Two additional but volumetrically minor styles of mineralization comprise (1) sphalerite-cemented stockwork breccia zones adjacent to the Jabiru fault (Fig. 9F), and (2) crosscutting, coarse-grained, pyrite-quartz-carbonate ± sphalerite, galena veins (Figs. 7E, 9J).

Mineralization in the Main lens is up to 31 m thick in the easternmost sector of the study area. The dominant mineralization style comprises fine-grained sphalerite (sp1) cement in the carbonaceous mudstone, accompanied by subordinate galena (gn1) and pyrite (py2). The pyrite content is vertically zoned in the Main lens, progressively increasing upward from a pyrite-poor lower portion (<7% py), to a central sphalerite-dominant portion (avg 15% py), to an upper pyrite-dominant portion (up to ~25% py). The Zn/Pb ratio averages ~6.5 and is relatively consistent in the Main lens across the deposit, both vertically and laterally. Main lens mineralization also contains minor pyrrhotite (~4%), and trace arsenopyrite and marcasite. Silver grades are unusually low, averaging <3 ppm across the deposit with no apparent zonation. The lack of Ag at Teena contrasts with HYC which averages 41 g/t Ag (Large et al., 1998).

Mineralization in the Lower lens is texturally and compositionally like the Main lens but has less total pyrite (avg <7%) and greater mesoscopic dolomite replacement-style mineralization, due to the higher proportion of dolomite nodules in the host rocks (e.g., Fig. 7C, D). Zinc grades are typically

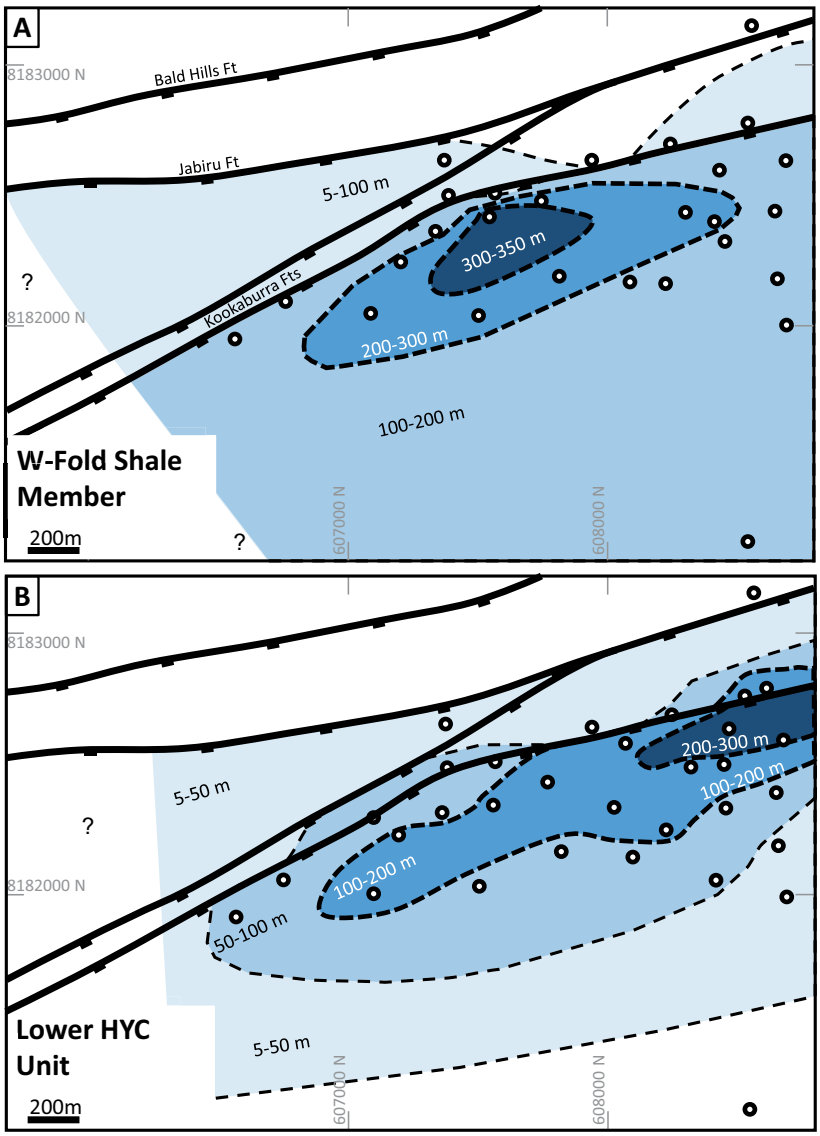


Fig. 6. Stratigraphic isopach thickness contour maps for (A) W-Fold Shale Member and (B) Lower HYC unit of the Barney Creek Formation.

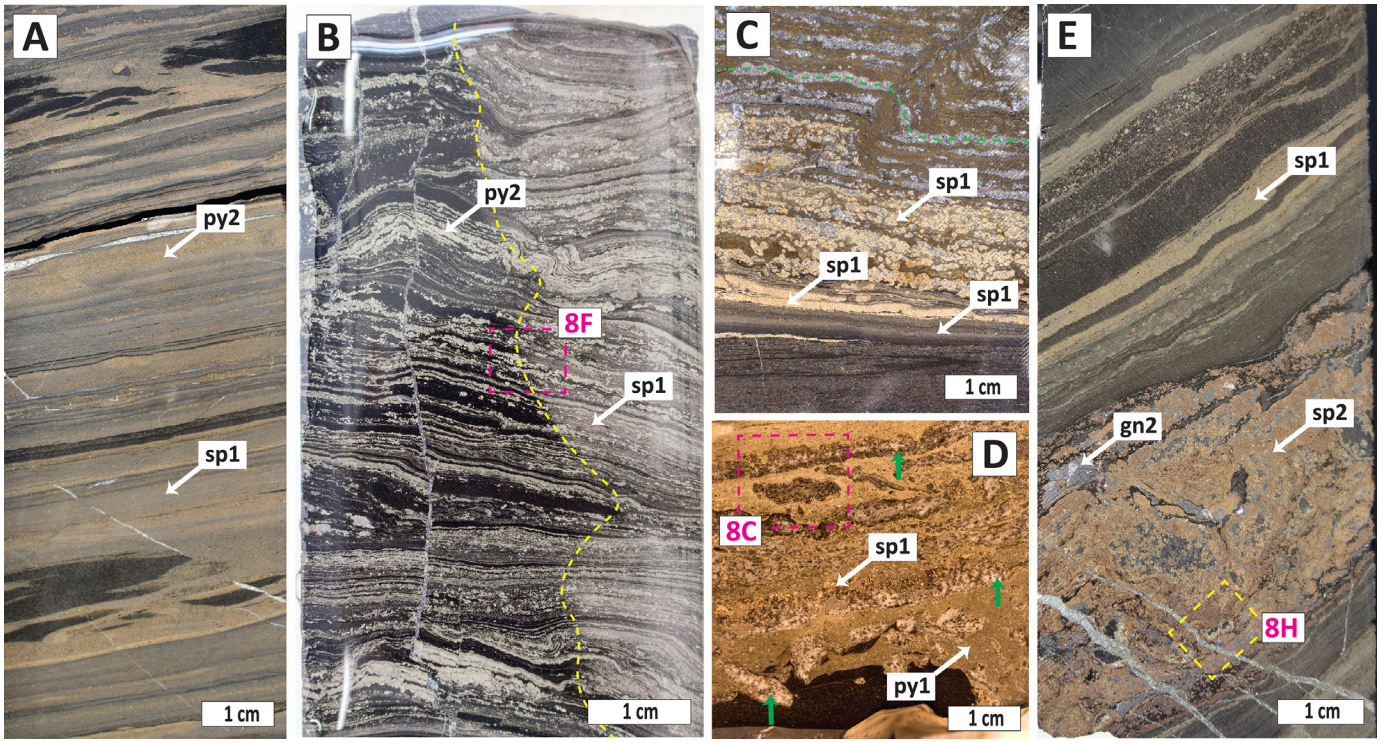


Fig. 7. Representative examples of stratiform Zn-Pb mineralization from the Main and Lower mineralization lenses in the Lower HYC unit. A. Semimassive sphalerite and pyrite laminae in the Main lens (TNDD010). Note irregular black remnants of unmineralized host rock enveloped by anastomosing mineralization seams in which sphalerite (sp1) forms fine-grained cement to a fine-grained carbonaceous mudstone. B. A transgressive mineralization replacement front in which the fine-grained sphalerite (sp1) cement at right stops abruptly at a high angle to bedding (TNDD025). Coarser-grained py2 overprints fine-grained py1a in and beyond the sp1 replacement front. The pink box highlights the area shown in Figure 8F. C. Sphalerite selective replacement of small dolomite nodules in the Lower lens (TNDD010). This sample preserves an intraformational microshear and drag fold (green dashed line highlights displacement) about which sphalerite (sp1) is asymmetrically distributed. D. Irregular dolomite nodules in a highly pyritic mudstone from the Lower lens (TNDD019). Weak sphalerite (sp1) selectively replaced some dolomite nodules (green arrows). Pink box highlights the area shown in Figure 8C. E. Strata-bound sphalerite (sp2) and galena (gn2) replacement vein in the Lower lens (TNDD019 @ 1,080 m). Pink box highlights an example of sealed dissolution cavities shown in Figure 8H.

slightly lower than in the Main lens and tend to be highest at the top of the Lower lens. The thickness of the Lower lens is broadly consistent at ~5 to 6 m in the east half of the deposit, thinning to <4 m toward the western margin. Galena is less abundant yielding a higher Zn/Pb ratio of ~8.5 across the Lower lens, and Ag grades are similarly very low (<2 ppm).

The dominant generation of sphalerite (sp1) in the Main and Lower lenses is tan to pale yellow in color and appears stratiform within individual laminations and thin beds, commonly reflecting the thickness and grainsize of individual siltstone or mudstone layers. Notably, there are frequent examples where sphalerite mineralization is transgressive to bedding, either anastomosing around millimeter- to centimeter-scale lenses of unmineralized carbonaceous shale (Fig. 7A) or, rarely, occurring as high-angle replacement fronts (Fig. 7B). Stratiform sphalerite can be texturally complex, ranging

Fig. 8. Close-up photographs of mineralization textures. A. Aggregates of py1a in wavy laminated mudstone and partially overgrown by a large dolomite nodule in Lower HYC unit. Compaction after nodule growth resulted in "pinch and swell" wavy laminations, whereas py1a inclusion trails in the nodule retains a more planar orientation (JM81 - TNDD019 @ 1,048 m). B. Py1b formed on the margins of a dolomite nodule in the Lower HYC unit beneath the Main mineralization lens (JM63 - TNDD019 @ 1,181 m). Py1a is abundant in specific laminae and there is partial selective replacement of dolomite micronodules by sp1 toward the bottom half of the image. C. Minor replacement of the margins of partially silicified dolomite nodules by tan (sp1) and red-brown (sp2) sphalerite. Remnant aggregates of py1a are disseminated in the dolomite nodule (JM78 - TNDD019 @ 1,069 m; Lower HYC unit). D. Sphalerite (sp1) replacement of dolomite micronodules concentrated along a lamination in the Lower HYC unit. The sphalerite also forms fine-grained cement in the mudstone host rock in the upper part of the image (JM73 - TNDD019 @ 1,107 m). E. Strata-bound aggregates of hydrothermal pyrite (py2) variably cemented by fine-grained sphalerite (sp1) in Lower HYC unit (JM155 - TNDD012 @ 676 m). F. Transgressive sphalerite (sp1) replacement of strata-bound pyrite (py1a, py2) and fine-grained mudstone matrix in the Lower HYC unit. The dashed yellow line marks the replacement front (JMX025 - TNDD025 @ 730 m). G. An irregular dolomite nodule partially replaced by two consecutive generations of sphalerite in the Lower HYC unit (JM79 - TNDD019 @ 1,064 m). H. Coarse-grained sphalerite (sp2) mineralization intergrown with interstitial galena (gn2) and with minor dissolution cavities filled by quartz and sphalerite, showing geopetal textures (JM73 - TNDD019 @ 1,080 m; Lower HYC unit).

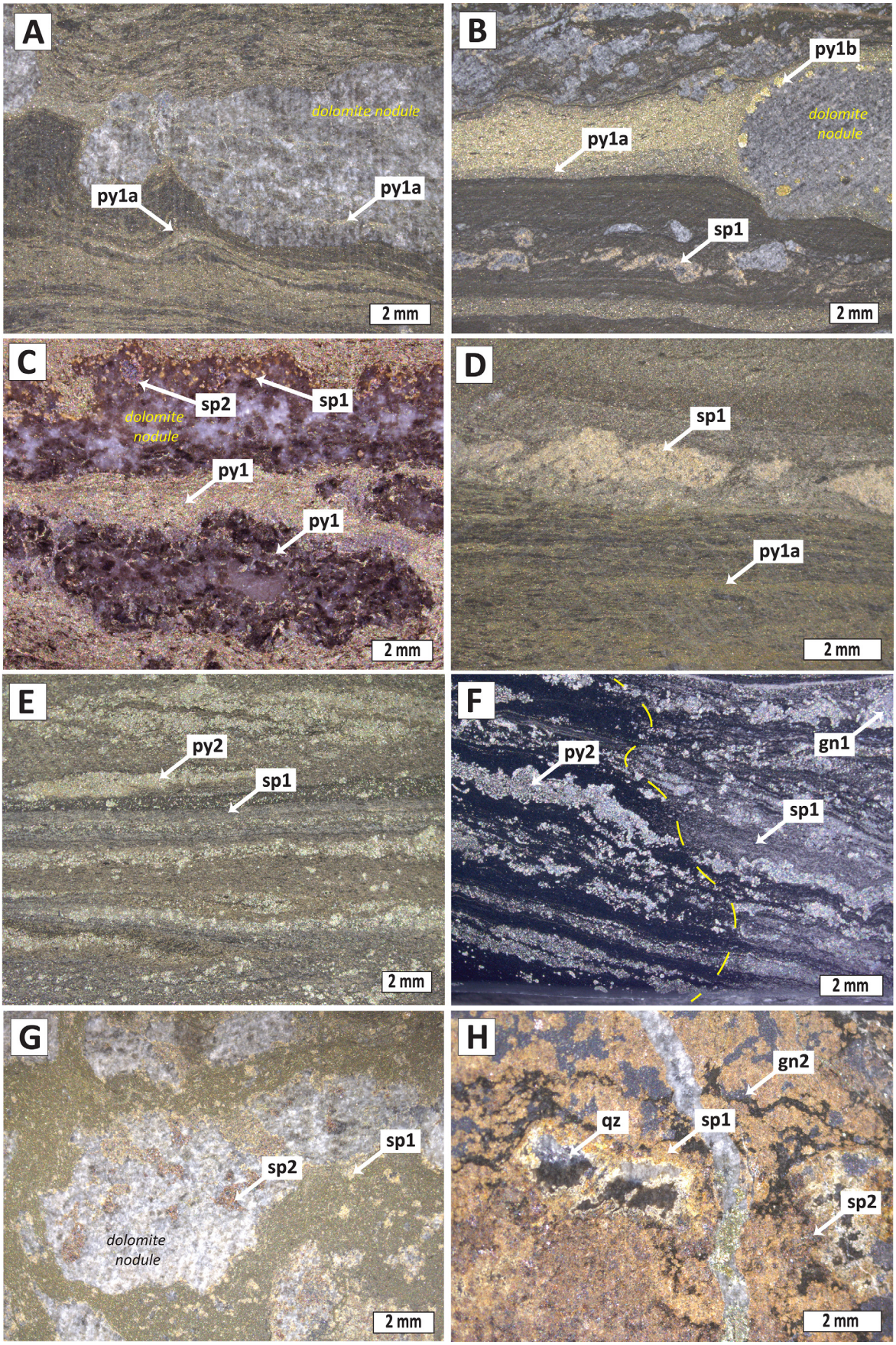

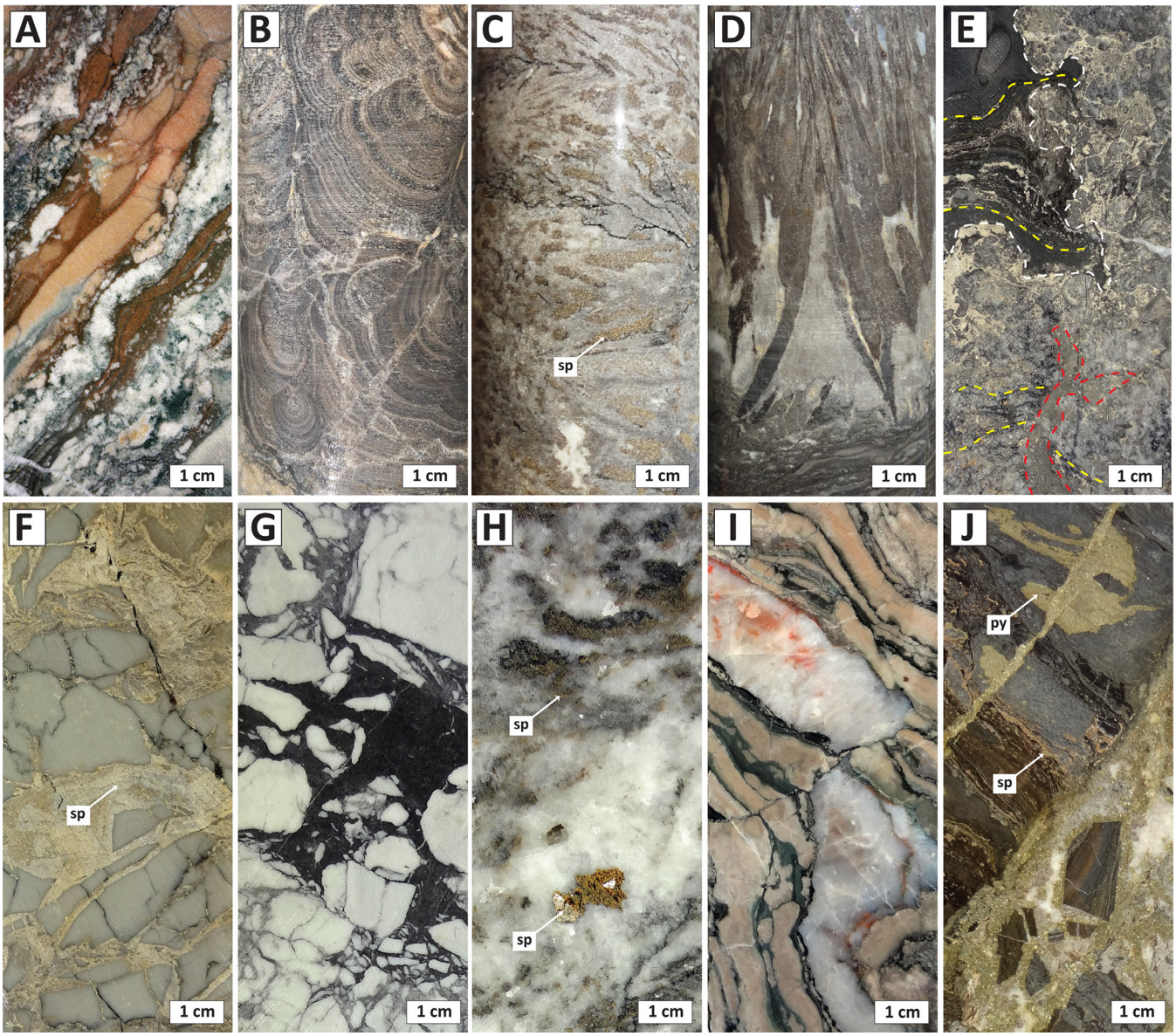


Fig. 9. Hand sample photographs of HTD and vein assemblages. A. Partial secondary dolomite (±quartz) replacement of nodular dolostone beds in the W-Fold Shale Member (TNDD015 @ 772 m). B. Botryoidal HTD (TNDD033 @ 1,025.5 m). C. Sideways radiating bladed dolomite with interstitial sphalerite and quartz (TNDD014 @ 705 m). D. Downward radiating fan of coarse HTD blades (after aragonite) with interstitial dolomite (TNDD017 @ 903.4 m). E. Massive HTD replacement with interstitial sphalerite and pyrite mineralization overprinting laminated pyritic carbonaceous shale from middle W-Fold Shale Member. Yellow dashed line shows relic bedding traces (TNDD11A @ 1,118 m). F. Sphalerite-cemented hydrothermal breccia (poststylobreccia) in Teena Dolostone from Jabiru fault zone (Teena4 @ 800 m). G. Black-matrix dolomite jigsaw to rubble breccia in Teena Dolostone (poststylolite; TNDD008 @ 639 m). H. Stockwork ankerite veining overprinting HTD (TNDD015 @ 831 m). I. Late-stage bedding-parallel quartz vein with trace hematite in W-Fold Shale Member (TNDD014 @ 1,104 m). J. High-angle late-stage quartz-carbonate-pyrite veins cutting mineralized Lower HYC unit (TNDD014).

from irregular masses of fine- (~10 $\mu$m) to medium-grained (~1 mm), subhedral to anhedral crystals that typically occur interstitial to py1 and py2, or in separate nonpyritic laminae and bands. Sphalerite also occurs in medium-grained, disseminated, tan-colored aggregates that partially replace dolomite nodules (Fig. 7C, D). Galena forms cryptocrystalline crystals interlaminated with sphalerite (sp1). Mineralization-stage pyrite (py2) is distinguishable from premineralization pyrite (py1) by coarser grain sizes (> 50 $\mu$m), which are commonly subhedral to spherical and occur as stratiform aggregates (Fig. 7B), along with centimeter-scale bands of disseminated sphalerite in pyritic carbonaceous siltstone beds (Fig. 7A).

A second generation of coarse-grained (0.5–2 mm) red-brown sphalerite (sp2), which is volumetrically minor, occurs with coarse-grained (0.5–5 mm) euhedral galena (gn2) and pyrite (py3) in 1- to 10-cm-thick bedding-parallel bands (Fig. 7E) that overprint the early sphalerite laminae (sp1). These vein-like bands are associated with abundant small (0.1–15 mm) dissolution cavities that are variously lined with sulfide

crystals and filled with quartz-dolomite-sulfide (± pyrobitumen) assemblages (Fig. 8H).

Footwall lens mineralization is hosted in the middle of the underlying W-Fold Shale Member and comprises two distinct styles of mineralization: (1) fine-grained stratiform sphalerite mineralization hosted in dolomitic carbonaceous siltstone beds (Figs. 10, 11A); and (2) strata-bound dolostone-hosted mineralization comprising interstitial aggregates, blebs, and stringers of medium-grained sphalerite with subordinate galena (Figs. 9C, E, 10, 11D). The stratiform mineralization style is thickest in the central and northeast portion of the deposit, and similar to, but lower grade and significantly less continuous laterally and vertically than the Lower and Main lenses. The dolostone-hosted mineralization occurs in a series of strata-bound massive hydrothermal dolomite (HTD) lenses (described below) that postdate the stratiform mineralization (Fig. 3C) and have an aggregate thickness of up to 200 m. It represents a newly identified style of mineralization for the region and is described in more detail below. Combined, the stratiform and dolostone-hosted mineralization grade ranges from 1.0 to 3.5% Zn + Pb over intervals typically 1 to 30 m thick (and up to 89 m thick).

*HTD alteration*

The footwall strata-bound HTD lenses represent a completely different style of sulfide mineralization to the stratiform mineralization in the Main and Lower mineralization lenses, one that is not commonly recognized in CD-type deposits. Two styles of HTD alteration are present in the Teena subbasin: (1) mineralized strata-bound HTD lenses in the W-Fold Shale Member (Figs. 3C, 10), and (2) unmineralized black-matrix breccias in the Teena Dolostone adjacent to the Jabiru fault (Figs. 3C, 9G). The multiple thin strata-bound lenses of massive HTD are distinguished from primary dolostone beds by their texturally destructive, replacement, and cavity-infill textures (Fig. 9). Up to four stacked lenses of this unit have been mapped, but typically there are only two main lenses present in each cross section (Fig. 3C). The lenses are semicontinuous and range in thickness from 1 to 30 m, with strike lengths and widths up to a few hundred meters. They locally crosscut the stratiform Footwall lens mineralization and tend to migrate up sequence from east to west, and to thicken from south to north toward the Jabiru fault.

Centers of the thicker HTD lenses have open-space cavity fill textures that include fans of radiating bladed dolomite with interstitial quartz and medium-grained interstitial tan to yellow sphalerite (Figs. 9C, D, 12), as well as irregular lobate margins and botryoidal growth (Fig. 9B). There are at least three stages of dolomite alteration at the centers of the dolostone lenses: (1) fine-grained dolomite associated with disseminated yellow sphalerite (sp2), which formed predominantly by matrix replacement and postdated laminated pyrite and sphalerite mineralization in the W-Fold Shale Member (Fig. 12A, B); (2) variably mineralized cavity-infill dolomite and quartz, commonly with bladed crystals up to 8 cm in length (Figs. 9C, D, 12B, C) and local botryoidal growth textures (Fig. 9B); and (3) sulfide-poor, coarse-grained dolomite-quartz replacement and infill (Fig. 12C). The dolomite blades typically exhibit a pseudohexagonal section, which indicates they are likely to have replaced aragonite crystals. In many cases the blades form downward- and sideway-radiating fans, which clearly distinguishes them from the ubiquitously upward-divergent Coxco needles and indicates an origin by open-space fill rather than seafloor evaporite growth.

There is little evidence for solution collapse breccias above the HTD lenses despite the evidence for extensive whole-rock dissolution. Rather, the HTD lenses are commonly bracketed by broad intervals (2–50 m thick) of partially recrystallized primary dolomite nodules, which extend farther south along the same horizons across the Teena subbasin, and

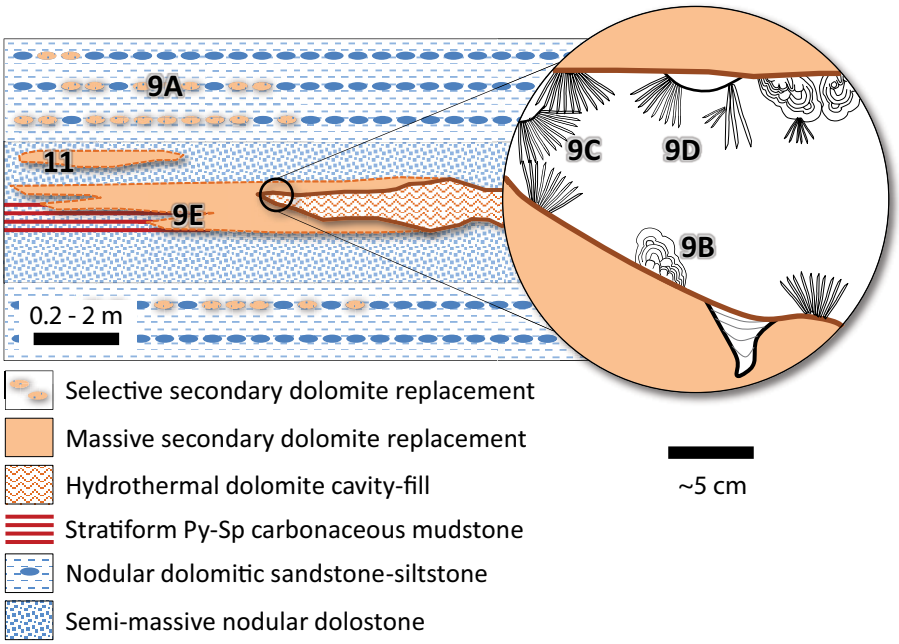


Fig. 10. Schematic interpretation of the textural zonation in hydrothermal dolomite (HTD) lenses from the W-Fold Shale Member, showing relative position of close-up photographs in Figures 9 and 11.

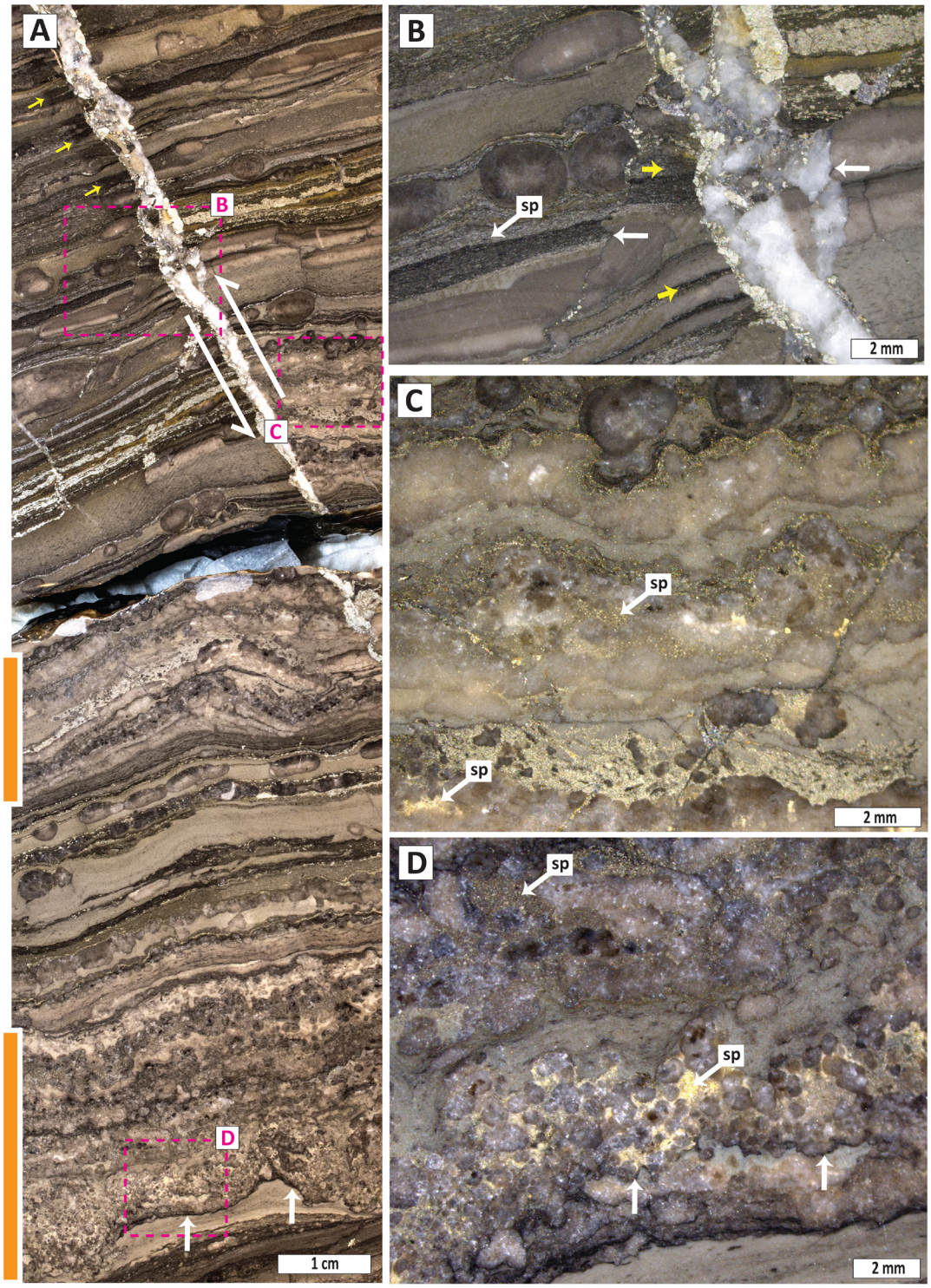


Fig. 11. A sample of the W-Fold Shale Member that preserves key paragenetic relationships among stratiform sphalerite mineralization and HTD (hydrothermal dolomite) mineralization. A. Beds of partial HTD replacement with mineralization are annotated (orange bars). A synorogenic quartz-carbonate-sulfide shear vein occurs in the upper half of the sample shows minor (~2 cm) offset of beds and a narrow wall-rock halo of depletion of stratiform sphalerite (sp1) mineralization (yellow arrows). The pink boxes highlight areas shown in (B) to (D) at higher resolution. B. Weak stratiform sphalerite (sp1) mineralization occurs as cement in carbonaceous laminations, with yellow arrows highlighting where sphalerite has been leached from the halo to the late vein. White arrows highlight stylolites that crosscut the stratiform mineralization (left-hand side) but borders the vein. C. Weak sphalerite (sp2) mineralization hosted by the massive HTD-quartz-sulfide band that selectively replaced a bed of diagenetic dolomite nodules. D. Another example of sphalerite (sp2) mineralization that is interstitial in a bed of recrystallized diagenetic dolomite micronodules (replaced by secondary dolomite and quartz), with stylolites (white arrows) toward the lower half of the image forming an impermeable boundary.

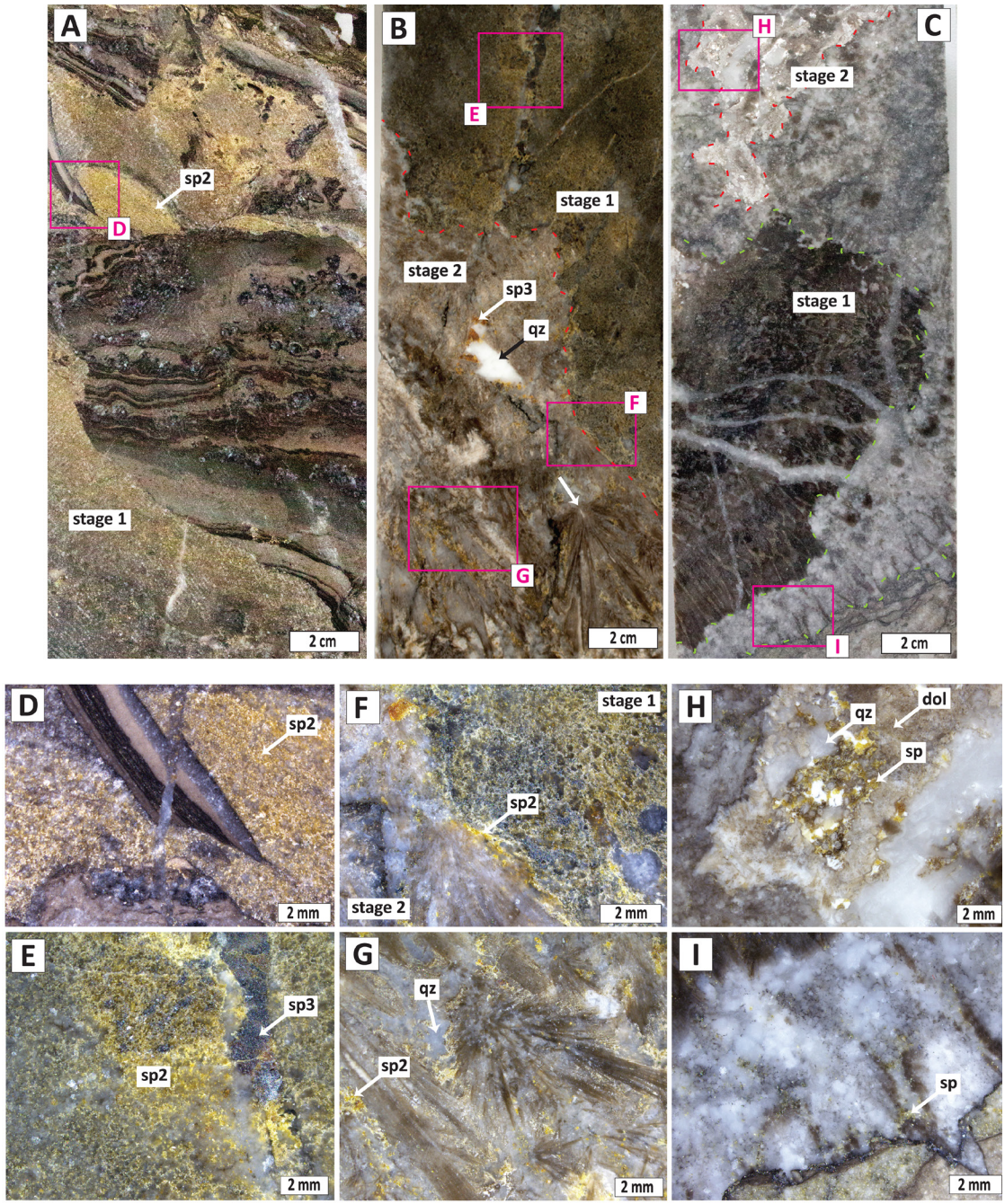


Fig. 12. Hand specimen photographs of the HTD (hydrothermal dolomite) lenses (A) to (C), with high-resolution binocular microscope images of areas highlighted in the pink boxes. A. Stage 1 strongly mineralized HTD-cemented breccia from middle W-Fold Shale Member. Fine-grained yellow sphalerite (sp2) mineralization is disseminated throughout both replacement and infill HTD (JM33 - TNDD015 @ 800 m). B. Stage 2 weakly mineralized hydrothermal bladed dolomite and quartz cavity-fill formed after dissolution of stage 1 dolomite (dashed red line shows dissolution boundary). Downward diverging needle fans in lower section of the image (white arrow) are associated with interstitial quartz (qz) and sphalerite (sp3) (JM32 - TNDD015 @ 802 m). C. Replacement of stage 2 hydrothermal bladed dolomite infill by stage 3 white dolomite-quartz assemblage (green dashed line shows replacement front), with subsequent dissolution resulting in irregular cavity infill by later stage silica and dolomite (red dashed line) (JM37 - TNDD015 @ 784 m). D. A close-up image of sphalerite (sp2) mineralization associated with stage 1 dolomite. An angular dolomitic carbonaceous siltstone fragment in the center of the image is crosscut by a late-stage dolomite vein. E. A close-up image of stage 1 sphalerite (sp2) mineralization crosscut by a late-stage vein containing dark brown sphalerite and dolomite. F. Dissolution contact between stage 1 and 2 HTD (labeled), in which sphalerite mineralization is clearly concentrated in the earlier stage 1. G. Fan of acicular needles of dolomite (arrow) formed in stage 2 with interstitial quartz (qz) and sphalerite (sp3). H. Cavity infill of stage 3 dolomite, filled by dolomite (dol), quartz (qz), and sphalerite (sp). I. Stage 3 dolomite with minor ghost bladed texture with sphalerite from preexisting stage 2 dolomite alteration, largely replaced by secondary dolomite and quartz. Stylolite along the bottom of the image forms a clear barrier to fluid flow during stage 2.

in separate strata-bound alteration zones. Dolomite recrystallization comprises patchy to complete replacement of the fine-grained, pale red (hematite-dusted) to light-gray dolomite nodules by aggregates of clean, white, coarser grained dolomite with minor quartz (Fig. 9A).

The fault-related hydrothermal black-matrix breccias occur as steeply dipping lenses up to several meters wide. From margin to core, textures transition from crackle to jigsaw to matrix-cemented chaotic breccia textures, with gray to black, fine-grained dolomite cement (Fig. 9G). Dolomite cement occurs as both dissolution infill and replacement among monomict angular dolostone clasts. No mineralization or sulfides have been observed in the matrix of these breccias. They postdate an earlier generation of minor white colloform-banded dolomite-quartz veins and are truncated updip by unconformable onlap of the Upper HYC unit in the footwall to the Jabiru fault.

*Late-stage veins*

A diverse suite of late-stage hydrothermal veins occurs throughout all members of the Barney Creek Formation, and to a much lesser extent the Teena and Reward Dolostone Formations at Teena. These veins crosscut stratiform Zn-Pb mineralization and bedding-parallel stylolites. We classify these veins into three main sets based on mineralogy and relative timing (Fig. 13): (1) ankerite veins, (2) quartz-hematite veins, and (3) quartz-carbonate-sulfide veins.

*Ankerite veins:* Ankerite veins are locally present in the W-Fold Shale Member where they frequently overprint HTD lenses, but also occur separately. They comprise irregular to planar, strata-bound arrays of vein stockworks and vein breccias filled with white, coarse-grained ankerite, minor sphalerite, and quartz (Fig. 9H). Locally these veins have vugs lined with coarse honey- to dark-brown-colored sphalerite crystals. Most veins are <10 cm thick, but where intensely developed, ankerite forms the cement to strata-bound jigsaw breccia lenses up to 10 m wide.

*Quartz-hematite veins:* Quartz-hematite veins are volumetrically minor and restricted to the W-Fold Shale Member at Teena. They comprise 0.1- to 3-cm-thick, irregular, bedding-parallel veins of quartz infill and silica replacement of dolomite and are typically associated with narrow, brick-red, disseminated hematite inclusions and alteration halos (Fig. 9I). They are frequently associated with small-scale bedding deformation, such as irregular open folds and mesoscopic faults, consistent with formation during an early episode of subhorizontal shortening.

*Quartz-carbonate-sulfide veins:* Quartz-carbonate-sulfide veins are volumetrically minor but widespread throughout the Barney Creek Formation and, to a much less extent, also the lower Reward Dolostone and W-Fold Shale Member at Teena. They comprise late-stage, planar to stockwork, shear vein sets with moderately steep dips and centimeter-scale reverse throw (refer to the "subbasin architecture and deformation section"), which are 0.1 to 5 cm thick and filled with highly variable proportions of medium- to coarse-grained calcite, dolomite, quartz, pyrite, sphalerite, and galena (Fig. 9J). Sulfides rarely occur in this vein set below Footwall lens mineralization but are common above the Main and Lower lenses.

## Discussion

*Growth fault propagation and structural evolution*

There is strong evidence that deposition of the Barney Creek Formation was controlled by the development of a half-graben structure during evolution of the Teena subbasin. Extreme asymmetry is observed in thickness changes among units of the Barney Creek Formation, which collectively thicken from ~270 m on the south limb of the Teena syncline, to a maximum thickness of 900 m in the subbasin depocenter, to <50 m in the footwall to the Jabiru fault. Extensional growth fault movement was initiated during deposition of the W-Fold Shale Member and persisted episodically until a weak structural disconformity developed in the Upper HYC unit within the Teena subbasin (Fig. 5). North of the subbasin, in footwalls to the Jabiru and Bald Hill fault zones, tilted and partially exhumed blocks of Teena Dolostone and Emmerugga Dolostone are unconformably overlain by Middle to Upper HYC units in a karstic platform, marking the cessation of this episode of extensional faulting by the time of Upper HYC deposition. Volumetrically minor sedimentary breccias of Teena Dolostone, near the base of the Middle HYC unit, indicate that limited erosional degradation of a footwall scarp occurred by the time of mid-HYC deposition.

The Jabiru fault had the strongest influence on syndepositional thickening of the W-Fold Shale and HYC Pyritic Shale members, as well as on the thickness and grade of the three principal mineralized horizons present in the Teena deposit (Figs. 6, 14). The pattern of eastward depocenter migration among the W-Fold Shale Member and Lower HYC unit suggests that the Kookaburra fault may have initially developed as part of a segmented relay fault system together with the Jabiru and Bald Hills faults (Fig. 6). Fault movement along the northern margin of the Teena subbasin ceased during deposition of the Upper HYC unit, when a marine regression returned the subbasin to stable carbonate platform sedimentation underlain by a cryptic structural disconformity internal to the subbasin.

Rotation of the footwall fault blocks between the Jabiru and Bald Hills faults in toward the subbasin is consistent with development of a growth syncline that was further tightened by later tectonic inversion. Two possible mechanisms for development of an extensional growth syncline are envisaged: (1) hanging-wall drag folding along a downward steepening "antilistric" normal fault, or (2) footwall block rotation between two or more synthetic normal faults (e.g., Ferrill et al., 2005). Given that the bedding dips southward on both sides of the Jabiru fault, we propose that the Teena growth syncline formed by a combination of both processes (Fig. 14). Minor steep N-dipping faults along the south limb of the Teena subbasin developed as antithetic normal faults to accommodate hanging-wall block rotation and subsidence.

*Lithofacies evolution*

Before the main episode of fault-controlled subsidence, deposition of the Teena Dolostone occurred in a shallow-water setting, typical of elsewhere in the southern McArthur Basin (Kunzmann et al., 2019). The rare algal laminations and stromatolitic textures preserved in the Teena Dolostone are consistent with deposition in a shallow intertidal (e.g., Ahmad

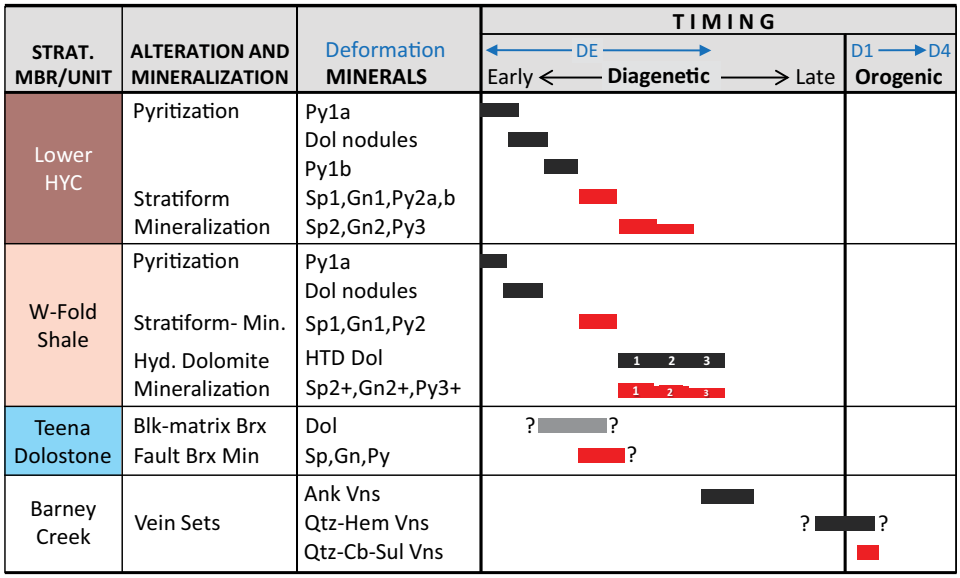


Fig. 13. Teena mineralization and alteration paragenesis. Refer to text for mineral abbreviations and paragenetic stages. Additional abbreviations: Blk-matrix Brx = Black-matrix breccia, fault Brx Min = fault breccia mineralization, Vns = veins, DE = extensional deformation, regional orogenic deformation events (D1-D4).

et al., 2013) to supratidal environment (Jackson et al., 1987), albeit one that may have been slightly deeper water than described elsewhere to account for the absence of evaporitic Coxco needle textures (Pietsch et al., 1991) and greater than average depositional thickness.

With the onset of tectonically controlled subsidence, deposition in the Teena subbasin transitioned to facies typical of deeper subtidal to slope environments as recorded by the Barney Creek Formation. The basal W-Fold Shale Member is a transitional lithology that comprises varying proportions of the dolostone and fine-grained dolomitic sandstone and siltstone end members of the Barney Creek Formation. Volcaniclastic sandstone beds, abrupt lithologic changes, flame structures, slump folding, and abrupt thickening of the W-Fold Shale Member toward the Kookabura fault, are all consistent with sedimentation in an unstable basin affected by syndepositional faulting along the northern subbasin margin. In contrast to the Teena subbasin where it is >250 m thick, the W-Fold Shale Member is no more than 60 m thick in the rest of the district. The intraformational small-scale folds, extensional microfaults and microthrusts with dominant north vergence in the W-Fold Shale Member can be linked to slump-related deformation processes (cf. Alsop and Marco, 2011). We speculate that formation of these slump features could have been triggered by episodic fault-induced tilting of poorly lithified beds toward the northern basin margin (Fig. 14). Similar small-scale intraformational structures with northeast vergence (downslope) also occur at the McArthur River (HYC) deposit (Hinman, 1995).

There is further evidence of tectonic instability in the Lower HYC unit, where graded volcaniclastic sandstone beds thicken into the subbasin depocenter and separate the two main mineralization lenses. These mass flow beds contain immature clasts of volcanogenic K-feldspar (Magnall et al., 2021) and may be compositionally similar to volcaniclastic units described elsewhere in the southern McArthur Basin (e.g., Davidson and Dashlooty, 1993). The presence of minor fault-proximal sedimentary breccias also provides evidence of more significant episodes of fault movement with local exhumation and degradation of footwall Teena Dolostone. In comparison to the McArthur River (HYC) deposit, however, there are no subbasin-wide sedimentary breccia beds present in the Teena subbasin and no unit equivalent to the fault-proximal Cooley Dolostone Member breccias. Furthermore, there is no evidence that sulfide mineralization was resedimented by the volcaniclastic sandstone beds in the Teena subbasin, as has been suggested at McArthur River (Ireland et al., 2004). These differences in abundance and style of the mass flow beds among the two subbasins are most likely related to contrasts in magnitude of footwall fault displacement, which is inferred to be less in the Teena subbasin and would have resulted in reduced footwall exhumation and erosion as well as lower energy sediment transport. The relationship among the volcaniclastic sandstone beds and sulfide mineralization at Teena is therefore the reverse to HYC, in that these mass-flow units predated mineralization and are not fault-proximal sedimentary breccias.

The Reward Dolostone is part of an overall upward-coarsening succession deposited in a shallow subtidal to peritidal environment with local sulfate evaporites (e.g., Jackson et al., 1987; Ahmad et al., 2013). A maximum regressive surface is developed near or at the top of the Reward Dolostone and is commonly expressed as a disconformity or unconformity associated with paleoweathering surfaces and karsts. Deposition of the Lynott Formation defines the next upward-deepening to upward-shallowing cycle, which transitioned from deep subtidal to shallow supratidal to sabkha facies (Jackson et al., 1987; Ahmad et al., 2013), also with common sulfate evaporite facies.

### *Mineralization paragenesis*

There are three intervals of sulfide mineralization in the Teena subbasin that are located at two stratigraphic levels in the

Barney Creek Formation (middle W-Fold Shale Member and Lower HYC unit). Overall, the Zn + Pb grades, thickness and continuity of mineralization increase upsequence. In the following discussion and summarized in Figure 13, the relative paragenetic timing of mineralization is interpreted with respect to host-rock deposition and regional deformation, then evaluated to determine whether sulfide mineralization in both stratigraphic levels corresponds to the same or separate hydrothermal events.

Evidence for replacement-style stratiform mineralization timing is observed across multiple scales. At the mesoscale, there are clear examples of discordant sphalerite (sp1) replacement fronts overprinting stratiform py1(Figs. 7B, 8F). The absence of apparent compaction-related thickness changes across these replacement fronts is consistent with timing that postdated early sediment compaction. Sphalerite mineralization also forms partial replacements of earlier generations of diagenetic dolomite nodules (Figs. 7C, 8D, G). The paragenetic relationships among py1, dolomite nodules, and sphalerite mineralization are particularly important to establish, considering they formed the basis for the SEDEX model at the nearby McArthur River deposit (e.g., Ireland et al., 2004). Notably, there are multiple examples of py1 trails overgrown by dolomite nodules (e.g., Fig. 8A), yet there are no comparable examples of this relationship with sphalerite. Rather, sphalerite mostly occurs in the interstitial spaces among aggregates of diagenetic pyrite and selectively replaces dolomite nodules. Both the cement and carbonate replacement modes of sphalerite are interpreted to be broadly coeval, as there are no obvious crosscutting or overprinting relationships (evidence also discussed in Magnall et al., 2021). All Zn-Pb mineralization at Teena postdated early diagenetic py1 and nodular dolomite growth, as well as early sediment compaction, and therefore, is considered to have formed mid to late diagenesis. Accordingly, Teena Zn mineralization is not cogenetic with fine-grained pyrite in the host rock, and there is no evidence here to support synsedimentary or syngenetic (SEDEX) timing for mineralization.

In the footwall stratigraphy to the Teena deposit, the HTD-hosted mineralization postdated early diagenetic hematite alteration (described in Magnall et al., 2021), the fine-grained stratiform mineralization, and bed-parallel stylolite formation (Figs. 11D, 12I). Within the mineralized HTD lenses there is evidence of extensive host-rock dolomite dissolution coupled with cavity-infill and replacement-style mineralization. Many of the dolomite crystal fans are top-nucleated and diverge downward or sideways (Figs. 9C, D, 12B), so they are distinctly different from the upward-divergent Coxco needle fans described elsewhere in the district in the Teena Dolostone (Coxco Dolostone Member; Pietsch et al., 1991). The downward growth, and common association with botryoidal dolomite textures, provides compelling evidence of open-space fill rather than seafloor evaporite growth. The dissolution zones are unlikely to be karstic cavities given their interpreted formation depth (Fig. 14B), their sill-like geometries, and their associated wall-rock alteration styles.

The relative timing of the different styles of dolomite-quartz-sulfide cavity fill, massive dolomite replacement, and secondary dolomite recrystallization is uncertain, but their close spatial relationship suggests that they are each paragenetically related (Fig. 10) and predated crosscutting syn-orogenic quartz-carbonate-sulfide veins. It is less clear how much of the HTD-hosted Zn mineralization was introduced by a separate pulse of mineralizing hydrothermal fluids or remobilized from earlier stratiform mineralization. Given that all HTD lenses are mineralized to some degree, and that the volume of dolomite-hosted mineralization exceeds footwall stratiform mineralization, we suggest that the timing of this event was late synmineralization with respect to the Main and Lower lenses and introduced new mineralization as part of a multiepisodic mineralization process. It is also suggested that the footwall HTD-hosted mineralization likely formed in association with the second-generation, coarse-grained mineralization event (sp2, gn2, py3) that overprinted the main stratiform mineralization lenses in the Lower HYC unit: both styles are associated with significant host-rock dissolution, quartz-dolomite infill, and coarse-grained Zn- (>Fe,Pb-) sulfide mineralization. The observation that secondary dolomite replacement both overprinted and was in-turn overprinted by layer-parallel stylolites supports a syndiagenetic formation timing.

### *Controls on mineralization*

*Lower HYC unit:* The highest mineralization grades in the Lower HYC unit are located close to the maximum throw on the subbasin-bounding faults (Figs. 3A, 6). As such, the Kookaburra and Jabiru faults appear to have been the principal feeder faults for all styles of Zn mineralization and hydrothermal dolostone lenses at Teena. The Jabiru fault is locally associated with mineralized hydrothermal breccia zones (Fig. 9F); however, these fault zones are mostly barren to only geochemically anomalous in Zn and Pb. Farther west, mineralization follows the syncline axis, proximal to the Kookaburra fault, but more distant to the Jabiru fault.

The stratiform mineralization is located >150 m (current thickness) below the MFS in the Middle HYC unit, which contains particularly high abundances of carbonaceous material and pyrite (Fig. 3B; Magnall et al., 2020). It has been suggested elsewhere that the most reducing facies (e.g., the MFS) should be targeted in SEDEX exploration models (e.g., Emsbo, 2009). Nevertheless, the Lower HYC unit does not represent the most reducing facies, as it contains a considerable amount of carbonate, where replacement of dolomite nodules clearly provided an important pathway of sulfide mineralization (e.g., Figs. 7, 8). Rather, mineralization in the Lower HYC unit broadly defines a major redox boundary between an oxidized hematite-stable footwall and a more reduced carbonaceous pyritic hanging wall.

Pyrite generations that are paragenetically linked to mineralization (py2) form overgrowths on py1 at least 200 m up into the hanging wall, as observed in drill holes TNDD012 and TNNDD019 (Magnall et al., 2020). The assumption is that py1 formed at or close to the sediment water interface, and so this mineralogical relationship indicates that Main lens stratiform mineralization formed at least 200 m below seafloor with respect to the present-day compacted thickness. In order to assess what the original depth of formation could have been before burial compaction of the host sequence, the 1st-order approximation method for sediment decompaction described by Angevine et al (1990) was applied. Following this method, it is inferred that the siltstone and mudstone

units in the Lower HYC unit were up to twice their current thickness upon deposition, whereas dolomitic siltstones and sandstones of the W-Fold Shale Member, the volcaniclastic sandstone beds, and Teena Dolostone were around 1.3 to 1.4 times thicker at deposition. Consequently, the minimum primary depth for the entire Teena mineralization sequence (Main, Lower, and Footwall lenses) likely ranged from >400 and <1,500 m below seafloor.

Our observations show that parts of the Kookaburra and Jabiru faults in the Lower HYC unit comprise only narrow semiductile deformation zones with little displacement, soft-sediment drag folding and clay smearing, and minor illite alteration. As such, the upper tips of these growth faults would have formed impermeable barriers to fluid flow (cf. Barnicoat et al., 2009). Furthermore, the partially lithified hanging-wall pyritic carbonaceous mudstone units may have acted as a cap rock seal that enhanced lateral intraformational fluid flow through the underlying more permeable carbonate-bearing Barney Creek Formation units.

These structural and lithologic observations can be combined to explain the paragenetic and stratigraphic relationships in the Teena subbasin (Figs. 13, 14). The earliest stages of subbasin development were associated with tectonic instability in the W-Fold Shale Member and Lower HYC unit but had no associated hydrothermal activity. Continued movement on the fault generated the accommodation space for the Middle HYC unit and deepening of the basin, as indicated by the MFS. Hydrothermal activity likely occurred during the terminal stages of growth faulting, which resulted in the development of one of the MFS higher up in the stratigraphy or followed shortly thereafter. The Lower HYC unit, which contained the reducing components (organic matter) for marine sulfate reduction, along with the dolomite cement and nodules that were susceptible to dissolution, would have been the first suitably permeable and reactive lithology encountered by an ascending hydrothermal fluid capable of promoting effective sulfide mineralization (Magnall et al., 2021). The conclusions reached here for the timing of stratiform Zn mineralization at the Teena deposit add to a growing number of studies that demonstrate that many large CD-type Zn-Pb deposits are not exhalative, but rather formed during burial diagenesis by subseafloor hydrothermal replacement and infill processes (e.g., Kelley et al., 2004; Reynolds et al., 2015; Maghfouri et al., 2019; Magnall et al., 2020; Spinks et al., 2021).

*Footwall mineralization:* The footwall HTD lenses represent a new style of mineralization not previously described in the Carpentaria Zn Province. There is clear evidence of multiple stages of carbonate dissolution and reprecipitation, resulting in a complex paragenesis and diverse styles of cavity infill textures (e.g., Figs 10, 12). Sphalerite is associated predominantly with the 1st stage of HTD formation as replacement of fine-grained dolomite. The 2nd stage of dolomite is associated with the dissolution of preexisting host rock and HTD, and destroys the grade of stage 1 sphalerite mineralization, but frequently hosts stage 2 interstitial sphalerite mineralization among coarse-bladed dolomite crystal fans (after aragonite). One or more stages of dissolution and more quartz-rich infill locally followed stage 2 and in several instances was further succeeded by late-stage ankerite stockwork veins. Mineralization grades in footwall HTD lenses decreased with successively younger paragenetic stages, whereas the quartz and Fe-in-carbonate contents increased, indicating waning input of mineralizing fluids and/or that less reduced sulfur was available for sulfide precipitation.

The style of HTD lenses present at Teena are similar to strata-bound HTD lenses frequently observed in Mississippi Valley- and Irish-type Zn-Pb-Ag deposits and many large petroleum reservoir facies around the world (Davies and Smith, 2006; Leach et al., 2010). Such HTD lenses developed in many sedimentary basins as structurally controlled, strata-bound, replacement and void-filling lenses, up to a few kilometers long and wide, in the hanging wall of intrabasinal extensional to wrench faults. Characteristic textures include zebra-dolomite, saddle dolomite, geopetal vug-fill, floating clast breccias and, less commonly, aragonite crystal fans and stalactites. The transient stability of dolomite in the HTD lenses likely records dynamic hydrogeochemical conditions. For example, it has been demonstrated through reactive transport simulation models that dolomite dissolution and reprecipitation requires fluid mixing among groundwater and acidic hydrothermal brines (Corbella et al., 2004). The stability of dolomite in reaction transport models requires brines that are saturated in Mg, where changes in key parameters (e.g., salinity, pH, $pCO_2$, and temperature) that arise from variable fluid mixing results in both dissolution and reprecipitation of dolomite (Anderson and Thom, 2008). This process could have occurred more commonly in the McArthur Basin than indicated by the published literature, although HTD is not always mineralized. For example, HTD-hosted mineralization has been observed at the Myrtle deposit (Agnew, 2005), and other occurrences in the basin may have been misinterpreted as primary dolostones.

Direct evidence of hydrothermal brines from fluid inclusion temperature and salinity constraints are currently lacking in the Teena subbasin, although it is possible to draw upon indirect lines of supporting evidence. Evaporative mineral phases (anhydrite and gypsum) and their pseudomorphs are extensively preserved in supratidal sabkha lithofacies of the River supersequence in the southern McArthur Basin (Kunzmann et al., 2019), meaning that there was likely active brine formation during this time. Indeed, brine formation has already been linked to the widespread K metasomatism in the Batten fault zone (Davidson, 1998; Magnall et al., 2021). Comparison can also be made to HTDs described elsewhere in the geologic record, which were typically deposited at shallow levels (<1,000 m deep) from moderately hot brines (80°–235°C) derived from evaporated seawater (bitterns), with salinities between 8 to 30 wt % equiv NaCl (Davies and Smith, 2006; Hollis et al., 2017).

The Zn-Pb sulfide mineralization that occurs in the HTD lenses in the Teena subbasin requires a source of reduced sulfur. Sulfate supplied from the brine could have been reduced during thermochemical sulfate reduction (TSR, reaction 1), or reduced sulfur may have been sourced directly from groundwater as $H_2S$ (reaction 2):

$$SO^{2-}_{4(aq)} + Zn^{2+} + CH_{4(aq)} = ZnS_{(s)} + H_2CO_3 + H_2O \quad (1)$$

and

$$H_2S_{(aq)} + Zn^{2+} = ZnS_{(s)} + 2H^+. \quad (2)$$

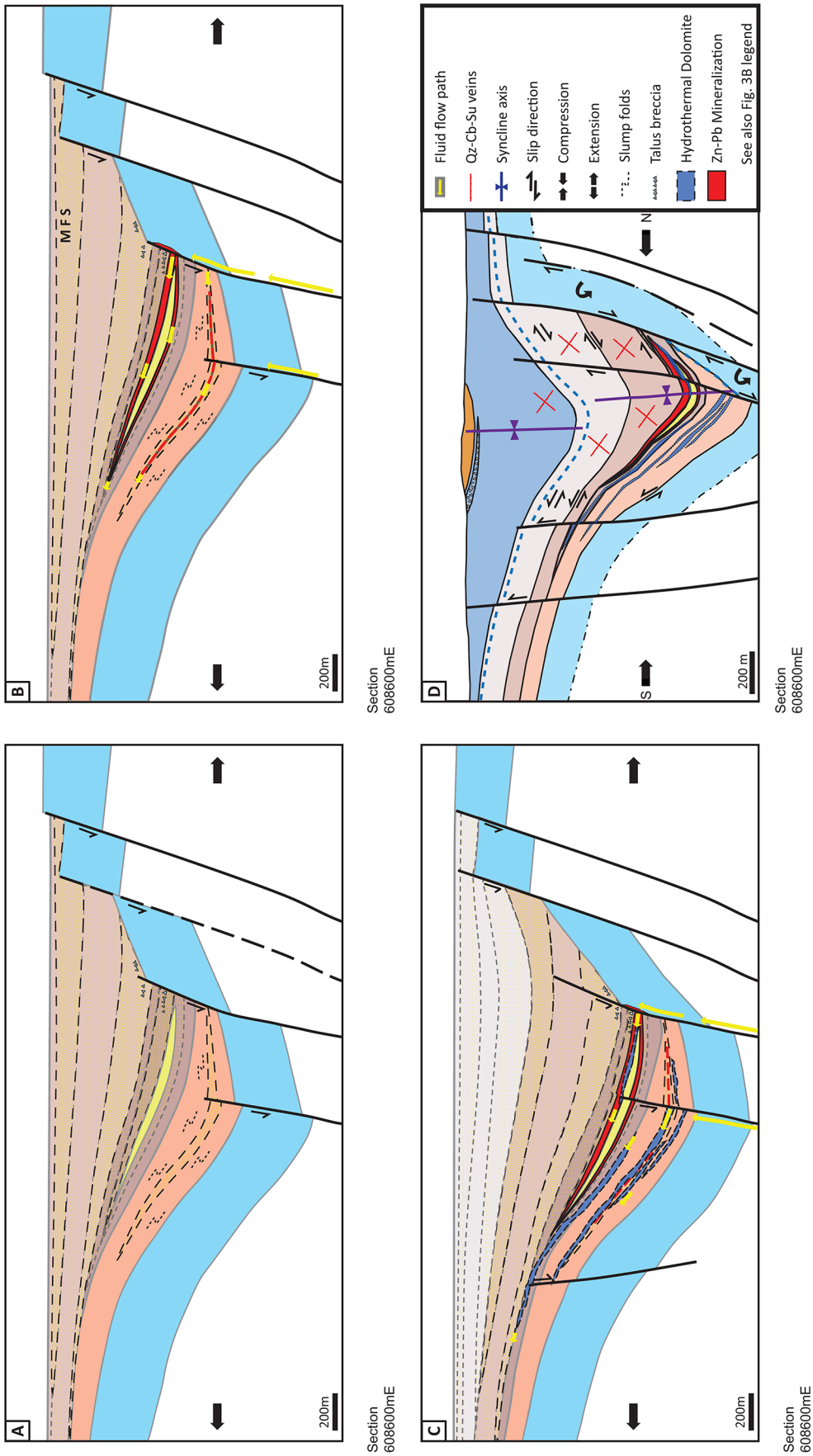


Fig. 14. Restored cross section (608600 mE, Fig. 3C) interpretations, showing proposed evolution of progressively decompacted sedimentary units during Barney Creek Formation deposition. A. Deposition of the Middle HYC unit with early diagenetic py1. B. Deposition of the Middle HYC unit and stratiform mineralization and py2. C. Deposition of the Upper HYC unit with py1, plus HTD (hydrothermal dolomite) alteration and mineralization. D. Syninversion deformation of $D_1$ Isan orogeny.

In reaction 1, the generation of $CO_2$ (or $H_2CO_3$) and reduced S by TSR results in much less dissolution than would result from simple mixing of aqueous sulfide in groundwater, or sour gas, and a hydrothermal metal-bearing solution (Corbella et al., 2004).

*Geodynamic controls on CD-type mineralization around 1640 Ma*

Although host-rock ages and inferred mineralization timing for CD-type Zn-Pb-Ag deposits in the Carpentaria Zn Province span 100 m.y., mineralization appears to have formed episodically from discrete events in time and space, likely associated with far-field tectonic triggers (e.g., Idnurm, 2000; Betts et al., 2003). It was recently proposed that several of these deposits formed during the 1650 to 1640 Ma Riversleigh Inversion Event and are linked to a regional shortening and inversion regime that drove fluid flow during subbasin evolution (Gibson et al., 2017). In the Teena subbasin, however, there is no evidence of syninversion deformation during the main stages of mineralization and HTD alteration. The only evidence for inversion-related mineralization at Teena is the late-stage quartz-carbonate-sulfide veins, which are interpreted to be a synorogenic conjugate vein set that formed during north-south horizontal ($D_1$) compression. These late-stage sulfide veins were derived predominantly by hydrothermal leaching and chemical remobilization of underlying sulfide mineralization and alteration (Fig. 11A).

There is widespread evidence that deposition of the River supersequence between 1645 to 1630 Ma was accommodated by a regional set of E- to ENE-trending synsedimentary growth faults in both the southern McArthur and northern Mt. Isa Basins (e.g., Bradshaw and Scott, 1999; Southgate et al., 2000; Betts et al., 2003; Bradshaw et al., 2018). Many of these faults possibly formed by reactivation of older, ENE-trending, synrift faults that developed during the early stages of the Calvert Superbasin between 1730 to 1700 Ma (Southgate et al., 2000; Betts et al., 2003). Several other mineralized subbasins that formed at a similar time to the Teena subbasin have similar fault geometries (Fig. 15), including subbasins that host the nearby McArthur River and Myrtle Zn-Pb deposits. The Walford Creek Cu-Zn-Co deposit and Bluebush Zn-Pb prospect in the Lawn Hill Platform (north-

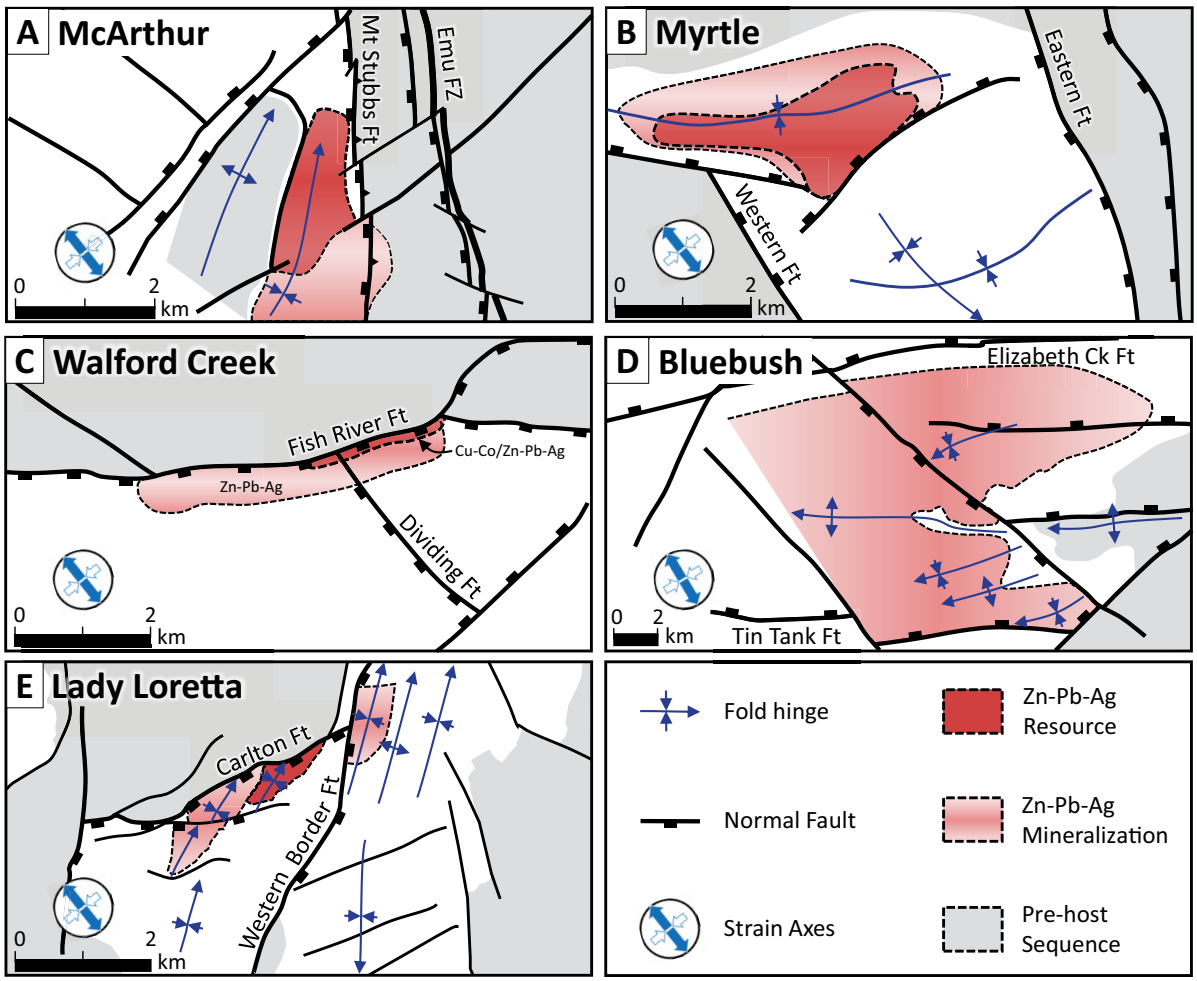


Fig. 15. Comparison of architecture of mineralized subbasins developed between 1647 to 1635 Ma across the northern Carpentaria Zn Province. A. McArthur (HYC) interpretation modified after Hinman (1995). B. Myrtle interpretation modified after Agnew (2005). C. Walford Creek interpretation modified after Rohrlach et al. (1998). D. Bluebush interpretation by Teck (unpub.). E. Lady Loretta interpretation modified after Large and McGoldrick (1998).

ern Mt. Isa Basin) are hosted by the respective Mount Les Siltstone (1640 ±7 Ma) and Riversleigh Siltstone (1644 ± 8 Ma; Page et al., 2000). The Lady Loretta Zn-Pb-Ag deposit, hosted by the Lady Loretta Formation (1647 ± 4 Ma; Page et al., 2000) in the Mt. Isa Basin, is a few million years older, but also occurs in a similar structural setting. Each of these CD-type deposits is broadly associated with two high-angle extensional growth fault sets that are oriented ENE to NE and NNW to NW (Fig. 15). In most cases, the ENE-NE extensional faults accommodated larger synsedimentary displacement than nearby NNW to NW faults, and more directly influenced subbasin architecture, lithofacies, and mineralization zonation.

It is evident that multiple deposits and prospects in the northern Carpentaria Zn Province formed around 1640 ±5 Ma in association with synsedimentary extensional growth faults. We interpret the dominant regional extension direction during formation of these deposits to have been oriented NNW-SSE, with subordinate ENE-WSW compression (Fig. 15), rather than north-south extension (e.g., McGoldrick et al., 2010) or NE-SW shortening and extension (Gibson et al., 2017). The most useful structural criteria for targeting these deposits are delineation of the primary ENE- and NNW-trending extensional fault sets, not pre-/synmineralization inversion structures.

Nevertheless, at the McArthur River deposit, it appears that localized inversion of the N-trending Mt. Stubbs fault did follow soon after mineralization ("Cooley Inversion" of Hinman, 1995), and this inverted fault is now partly overturned to yield a steep east dip. North of the McArthur River deposit, the upper Barney Creek Formation onlaps onto the inverted western fault block at a stratigraphic position similar to the upper Barney Creek Formation structural disconformity and unconformity observed in the Teena subbasin. This transient inversion event may be explained by waning of the short-lived NNW-SSE extensional phase, which permitted a brief reversion to ENE-WSW compression and resulted in localized inversion of some N- to NNW-trending faults (e.g., Wickens Hill fault). In contrast, ENE-trending faults likely remained largely transtensional due to their low angle to the principal shortening direction. Further inversion of N-S- and NNW-trending faults likely occurred during the principal $D_2$ east-west shortening event of the Isan orogeny. Dome and basin fold patterns in the Batten fault zone (Fig. 1B), as well as the diverse range of inverted subbasin orientations, further reflect the complex interaction of not just these NNW- and ENE-trending extensional fault sets, but also local reactivation of other older basement fault sets by $D_1$ north-south and $D_2$ east-west shortening during the Isan orogeny.

Both the relatively short-lived duration (<10 m.y.) and widespread extent (>150,000 km$^2$) of the 1640 ± 5 Ma mineralization event support interpretations that an abrupt regional tectonic trigger disrupted thermal subsidence-phase sedimentation of the River supersequence. The event coincides with a hairpin bend in the North Australia Apparent Polar Wander Path around ca. 1640 Ma (Fig. 2; Idnurm, 2000), which was almost certainly associated with far-field continental collision during assembly of the Nuna Supercontinent (e.g., Betts et al., 2016).

Our preferred model is that blanket coverage of synrift sediments by thermal subsidence phase sediments produced locally overpressured fluid reservoirs in thick synrift clastic sequences. Disruption of thermal subsidence by a weak north-northwest–south-southeast tectonic extension event, during which the River supersequence was deposited, produced steep extensional faults that locally tapped those fluid reservoirs, allowing rapid and episodic discharge of metal-rich hydrothermal fluids. This style of late-stage extensional faulting was characterized by low bulk strain, highly localized reactivation of favorably oriented (roughly colinear) Calvert-aged basement faults, and highly localized half-graben subbasin development. The importance of activation of local extension faults to drive the CD-type mineral system cannot be overstated: faulting not only breached source reservoirs and provided rare high flux-fluid conduits, but also created local metal trap environments along flow paths, which comprised deeper 4$^{th}$-order subbasin depocenters enriched in organic C and $S^{2-}$ reductants. Furthermore, tectonic tightening of fault-bound half-grabens into synclines facilitated structural preservation of shallow-level mineralization during orogenic basin inversion.

## Conclusions

1. The Teena deposit is hosted in the depocenter of a discrete 4$^{th}$-order subbasin that developed during deposition of the Barney Creek Formation (~1640 Ma) along the northern margin of the larger 3$^{rd}$-order Hot Spring-Emu subbasin.
2. Shifting patterns in depocenter location, sedimentary facies development, and mineralization and alteration zonation are attributed to progressive growth of an ENE-trending, synsedimentary, segmented fault zone and extensional half-graben depocenter.
3. Stratiform mineralization in the Lower HYC unit at Teena was deposited mid-diagenesis in a suboxic sedimentary facies well below the MFS, and at least 400 m below the paleosurface, after deposition of abundant and widespread early-diagenetic py1 and dolomite nodules.
4. Teena mineralization is partly cospatial but not cogenetic with its premineralization pyritic hanging wall.
5. Deposition of Teena stratiform mineralization resulted from flow of metalliferous hydrothermal fluids along the most permeable and reactive sedimentary host facies lateral to a growth fault conduit, below the level at which growth fault displacement appears to have terminated in and been effectively sealed by the hanging-wall carbonaceous mudstone.
6. Mineralization precipitated in primary and secondary pore spaces, and by carbonate replacement, upon reaction with $H_2S$-rich pore fluids derived from thermochemical sulfate reduction. Synmineralization acid production created secondary porosity through carbonate dissolution, which further enhanced lateral fluid flow with positive feedback.
7. Hydrothermal mineralization in each of three mineralized lenses resulted from a two-stage process that evolved from (1) early-stage, fine-grained, stratiform replacement, to (2) later stage, coarse-grained, infill and replacement mineralization associated with more extensive carbonate dissolution and dolomite-silica cavity infill and replacement. This transition was likely associated with influx of higher temperature and lower pH mineralizing fluids.
8. Strata-bound mineralized HTD lenses in the footwall W-Fold Shale Member resulted from multistage dolomite

dissolution, cavity-fill by dolomite (±silica, ±sulfide) and dolomite-silica replacement, driven by mixing of metalliferous hydrothermal brines with Ca-Mg-saturated, $H_2S$-bearing brines. Although not common to CD-type Zn deposits, HTD-style alteration and mineralization is common worldwide to many carbonate-hosted Zn-Pb-Ag deposits.

9. Subbasin development and syndiagenetic hydrothermal mineralization at Teena, and throughout the River supersequence across the northern Carpentaria Zn Province, are interpreted to have been geodynamically driven by a short-lived episode of north-northwet–south-southeast regional extension around ca 1640 Ma.

## Acknowledgments

We gratefully acknowledge funding for Joe Magnall's and Sarah Gleeson's research from Helmholtz-Rekrutierungsinitive. Teck funded the exploration work, with contributions from Rox Resources Limited in the early stages. Teck also supported internal research and provided permission to publish. We thank several Teck staff who contributed significant knowledge and review comments, including Iain Dalrymple, Darren Hunt, Andrew Davies, and James Botterill. We are also grateful to Neil Williams and Koen Torremans for their helpful review suggestions, which significantly improved the manuscript.

## REFERENCES

Agnew, M.W., 2005, Myrtle Sub-basin Final Report EL10316. Batten Joint Venture between Anglo American Exploration (Australia) Pty Ltd and Rio Tinto Exploration Pty Ltd., 59 p., available online at https://geoscience.nt.gov.au/gemis/ntgsjspui/handle/1/3

Ahmad, M., Dunster, J.N., and Munson, T.J., 2013, McArthur Basin, *in* Ahmad, M., and Munson, T.J., comps., Geology and mineral resources of the Northern Territory: Northern Territory Geological Survey Special Publication 5, chapter 15.

Alsop, G.I., and Marco, S., 2011, Soft-sediment deformation within seismogenic slumps of the Dead Sea Basin: Journal of Structural Geology, v. 33, p. 433–457.

Anderson, G.M., and Thom, J., 2008, The role of thermochemical sulfate reduction in the origin of Mississippi Valley-type deposits. II. Carbonate-sulfide relationships: Geofluids, v. 8, p. 27–34.

Angevine, C.L., Heller, P.L., and Paola, C., 1990, Quantitative sedimentary basin modeling: American Association of Petroleum Geologists Shortcourse Note Series 32, 247 p.

Barnicoat, A.C., Sheldon, H.A., and Ord, A., 2009, Faulting and fluid flow in porous rocks and sediments: Implications for mineralisation and other processes: Mineralium Deposita, v. 44, p. 705–718.

Betts, P.G., Giles, D., Lister, G.S. and Frick, L.R., 2002, Evolution of the Australian lithosphere: Australian Journal of Earth Sciences, 49(4), p. 661–695.

Betts, P.G., Giles, D., and Lister, G.S., 2003, Tectonic environment of shale-hosted massive sulfide Pb-Zn-Ag deposits of Proterozoic northeastern Australia: Economic Geology, v. 98, p. 557–576.

Betts, P.G., Giles, D., Mark, G., Lister, G.S., Goleby, B.R. and Aillères, L., 2006, Synthesis of the Proterozoic evolution of the Mt. Isa inlier: Australian Journal of Earth Sciences, v. 53, p. 187–211.

Betts, P.G., Armit, R.J., Stewart, J., Aitken, A.R.A., Ailleres, L., Donchak, P., Hutton, L., Withnall, I., and Giles, D., 2016, Australia and Nuna: Geological Society Special Publication. 424, p. 47–81.

Blevings, S.K., Kraft, J.L., Stemler, J.U., and Krolak, T.E., 2013, An overview of the structure, stratigraphy, and Zn-Pb-Ag deposits of the Red Dog district, Northwestern Alaska: Economic Geology Special Publication 17, p. 361–388.

Bradshaw, B.E., and Scott, D.L., 1999, Integrated basin analysis of the Isa Superbasin using seismic, well-log and geopotential data: An evaluation of the economic potential of the Northern Lawn Hill Platform: Australian Geological Survey Organisation Record 19, p. 1–173.

Bradshaw, B.E., Orr, M.L., Bailey, A.H.E., Palu, T.J., and Hall, L.S., 2018, Northern Lawn Hill Platform depth structure and isochore mapping update: Canberra, Geoscience Australia Record 2018/47, http://dx.doi.org/10.11636/Record.2018.047

Broadbent, C., Myers, R.E., and Wright, V., 1998, Geology and origin of shale-hosted mineralization at the Century deposit, Queensland, Eromanga: Economic Geology, v. 93, p. 1264–1294.

Carne, R.C., and Cathro, R.J., 1982, Sedimentary exhalative (sedex) zinc-lead-silver deposits, northern Canadian Cordillera: Canadian Institute of Mining Bulletin, v. 75, p. 66–78.

Cooke, D.R., Bull, S.W., Large, R.R., and McGoldrick, P.J., 2000, The importance of oxidized brines for the formation of Australian Proterozoic stratiform sediment-hosted Pb-Zn (Sedex) deposits: Economic Geology, v. 95, p. 1–18.

Corbella, M., Ayora, C., and Cardellach, E., 2004, Hydrothermal mixing, carbonate dissolution and sulfide precipitation in Mississippi Valley-type deposits: Mineralium Deposita, v. 39, p. 344–357.

Davidson, G.J., 1998, Alkali alteration styles and mechanisms, and their implications for a "brine factory" source of base metals in the rift-related McArthur group, Australia: Australian Journal of Earth Sciences, v. 45, p. 33–49.

Davidson, G.J,. and Dashlooty, S.A., 1993, The Glyde Sub-basin: A volcaniclastic-bearing pull-apart basin coeval with the McArthur River base-metal deposit, Northern Territory: Australian Journal of Earth Sciences, v. 40, p. 527–543.

Davies, G.R., and Smith, L.B., Jr., 2006, Structurally controlled hydrothermal dolomite reservoir facies: An overview: American Association of Petroleum Geologists Bulletin, v. 90, p. 1641–1690.

Duffett, M.L., Roach, M., and Leaman, D.E., 2007, Inferring central McArthur Basin shape at HYC time: Integration of geophysical interpretation and geology using GIS, *in* Munson, T. and Ambrose, G. eds., Proceedings of the Central Australian Basins Symposium, Northern Territory Geological Survey, Alice Springs, p. 22.

Emsbo, P., 2009, Geologic criteria for the assessment of sedimentary exhalative (sedex) Zn-Pb-Ag deposits: U.S. Geological Survey Open-File Report 1209, p. 21.

Etheridge, M.A., and Wall, V., 1994, Tectonic and structural evolution of the Australian Proterozoic [abs.]: Geological Society of Australia Abstracts, v. 37, p. 102–103.

Ferrill, D.A., Morris, A.P., Sims, D.W., Waiting, D.J., and Hasegawa, S., 2005, Development of synthetic layer dip adjacent to normal faults: American Association of Petroleum Geologists Memoir 85, p. 125–138.

Gibson, G.M., Hutton, L.J., and Holzschuh, J., 2017, Basin inversion and supercontinent assembly as drivers of sediment-hosted Pb-Zn mineralization in the Mount Isa region, northern Australia: Journal of the Geological Society, v. 174, p. 773–786.

Giles, D., Betts, P., and Lister, G., 2002, Far-field continental backarc setting for the 1.80–1.67 Ga basins of northeastern Australia: Geology, v. 30, p. 823–826.

Giles, D., Betts, P. Ailleres, L., Hulschur, B., and Lister, G., 2006, Evolution of the Isan orogeny at the southeastern margin of the Mt. Isa inlier: Australian Journal of Earth Sciences, v. 53, p. 91–108.

Gustafson, L.B., and Williams, N., 1981, Sediment-hosted stratiform deposits of copper, lead, and zinc: Economic Geology 75th Anniversary Volume, p. 139–178.

Hinman, M., 1995, Base metal mineralization at McArthur River: Structure and kinematics of the HYC-Cooley zone at McArthur River: Australian Geological Survey Organisation Record 1995/5.

Hollis, C., Bastesen, E., Boyce, A., Corlett, H., Gawthorpe, R., Hirani, J., Rotevatn, A., and Whitaker, F., 2017, Fault-controlled dolomitization in a rift basin: Geology, v. 45, p. 219–222.

Huston, D.L., Stevens, B., Southgate, P.N., Muhling, P., and Wyborn, L., 2006, Australian Zn-Pb-Ag ore-forming systems: A review and analysis: Economic Geology, v. 101, p. 1117–1157.

Idnurm, M., 2000, Towards a high resolution late Palaeoproterozoic-earliest Mesoproterozoic apparent polar wander path for northern Australia: Australian Journal of Earth Sciences, v. 47, p. 405–429.

Ireland, T., Large, R.R., McGoldrick, P., and Blake, M., 2004, Spatial distribution patterns of sulfur isotopes, nodular carbonate, and ore textures in the McArthur River (HYC) Zn-Pb-Ag deposit, Northern Territory, Australia: Economic Geology, v. 99, p. 1687–1709.

Jackson, M.J. and Southgate, P.N., 2000, Evolution of three unconformity-bounded sandy carbonate successions in the McArthur River region of

northern Australia: The Lawn, Wide and Doom supersequences in a proximal part of the Isa Superbasin: Australian Journal of Earth Sciences, v. 47, p. 625–635.
Jackson, M.J., Muir, M.D., and Plumb, K.A., 1987, Geology of the southern McArthur Basin, Northern Territory: Bureau of Mineral Resources, Geology and Geophysics Bulletin 220.
Jackson, M.J., Southgate, P.N., Winefield, P.R., Barnett, K. and Zeilinger, I., 2000, Revised sub-division and regional correlation of the McArthur Basin succession based on NABRE's 1995–8 sequence stratigraphic studies: Australian Geological Survey Organization Record 2000/3.
Jennings, S., and King, A.R., 2002, Geology, exploration history and future discoveries in the Red Dog district, western Brooks Range, Alaska: Giant ore deposits: Characteristics, genesis and exploration: Centre for Ore Deposit Research Special Publication 4, p.151–158.
Kelley, K.D., Dumoulin, J.A., and Jennings, S., 2004, The Anarraaq Zn-Pb-Ag and barite deposit, northern Alaska: Evidence for replacement of carbonate by barite and sulfides: Economic Geology, v. 99, p.1577–1591.
Krassay, A.A., Bradshaw, B.E., Domagala, J., and Jackson, M.J., 2000, Siliciclastic shoreline to growth-faulted, turbiditic sub-basins: The Proterozoic River supersequence of the upper McNamara Group on the Lawn Hill Platform, northern Australia: Australian Journal of Earth Sciences, v. 47, p. 533–562.
Kunzmann, M., Schmid, S., Blaikie, T.N., and Halverson, G.P., 2019, Facies analysis, sequence stratigraphy, and carbon isotope chemostratigraphy of a classic Zn-Pb host succession: The Proterozoic middle McArthur Group, McArthur Basin, Australia: Ore Geology Reviews, v. 106, p. 150–175.
Large, R.R., and McGoldrick, P.J., 1998, Lithogeochemical halos and geochemical vectors to stratiform sediment hosted Zn-Pb-Ag deposits. 1. Lady Loretta Deposit, Queensland: Journal of Geochemical Exploration, v. 63, p.37–56.
Large, R.R., Bull, S.W., Cooke, D.R., and McGoldrick, P.J., 1998, A genetic model for the HYC deposit, Australia: Based on regional sedimentology, geochemistry, and sulfide-sediment relationships: Economic Geology, v. 93, p. 1345–1368.
Large, R.R., Bull, S.W., McGoldrick, P.J., and Walters, S.G., 2005, Stratiform and strata-bound Zn-Pb-Ag deposits in Proterozoic sedimentary basins, northern Australia: Economic Geology, v. 100, p. 931–963.
Leach, D., Marsh, E., Bradley, D., Gardoll, S., and Huston, D., 2005, The distribution of SEDEX Pb-Zn deposits through Earth history, *in* Mao, J., and Bierlein, F.P., eds., Mineral deposit research: Meeting the global challenge: Berlin, Heidelberg, Springer, p. 145–148, doi. org/10.1007/3-540-27946-6_38.
Leach, D.L., Taylor, R.D., Fey, D.L., Diehl, S.F., and Saltus, R.W., 2010, A deposit model for Mississippi Valley-type lead-zinc ores: U.S. Geological Surve, Scientific Investigations Report 2010-5070-A, Mineral Deposit Models for Resource Assessment, 64 p.
Maghfouri, S., Hosseinzadeh, M.R., Choulet, F., Alfonso, P., Zadeh, A.M.A., and Rajabi, A., 2019, Vent-proximal sub-seafloor replacement clastic-carbonate hosted SEDEX-type mineralization in the Mehdiabad world-class Zn-Pb-Ba-(Cu-Ag) deposit, southern Yazd Basin, Iran: Ore Geology Reviews, v. 113, p. 103047.
Magnall, J.M., Gleeson, S.A., Hayward, N., and Rocholl, A., 2020, Massive sulfide Zn deposits in the Proterozoic did not require euxinia: Geochemical Perspective Letters, v. 13, p. 19–24.
Magnall, J.M., Hayward, N., Gleeson, S.A., Schleicher, A., Dalrymple, I., King, R., and Mahlstadt, N., 2021, The Teena Zn-Pb deposit (McArthur Basin, Australia). Part II. Carbonate replacement sulfide mineralization during burial diagenesis—implications for mineral exploration: Economic Geology, v. 116, p. 27–60..
McGoldrick, P., Winefield, P., Bull, S., Selley, D., and Scott, R., 2010, Sequences, synsedimentary structures, and sub-basins: the where and when of SEDEX zinc systems in the Southern McArthur Basin, Australia: Economic Geology Special Publication 15, p. 367–389.
Mudd, G.M., Jowitt, S.M., and Werner, T.T., 2017, The world's lead-zinc mineral resources: Scarcity, data, issues and opportunities: Ore Geology Reviews, v. 80, p. 1160–1190.
Neudert, M., and McGeough, M., 1996, A new tectonostratigraphic framework for the deposition of the upper McArthur Group, NT [ext. abs.]. James Cook University of North Queensland Economic Geology Research Unit, Extended Abstracts 55, p. 90–94.
Page, R.W., and Sweet, I.P., 1998, Geochronology of basin phases in the western Mt. Isa inlier, and correlation with the McArthur Basin: Australian Journal of Earth Sciences, v. 45, p. 219–232.
Page, R.W., Jackson, M.J., and Krassay, A.A., 2000, Constraining sequence stratigraphy in north Australian basins: SHRIMP U-Pb zircon geochronology between Mt. Isa and McArthur River: Australian Journal of Earth Sciences, v. 47, p. 431–459.
Pietsch, B.A., Rawlings, D.J., Creaser, P.M., Kruse, P.D., Ahmad, M., Ferenczi, P.A., and Findhammer, T.L.R., 1991, 1:250,000 Geological Map Series Explanatory Notes, Bauhinia Downs SE53-3.
Plumb, K.A., and Wellman, P., 1987, McArthur Basin, Northern Territory: Mapping of deep troughs using gravity and magnetic anomalies: Bureau of Mineral Resources Journal of Australian Geology and Geophysics, v. 10, p. 243–251.
Rawlings, D.J., Korsch, R.J., Goleby, B.R., Gibson, G.M., Johnstone, D.W., and Barlow, M., 2004, The 2002 Southern McArthur Basin Seismic Reflection Survey: Geoscience Australia, Record 17, 78 p.
Reynolds, M.A., Gingras, M.K., Gleeson, S.A., and Stemler, J.U., 2015, More than a trace of oxygen: Ichnological constraints on the formation of the giant Zn-Pb-Ag ± Ba deposits, Red Dog district, Alaska: Geology, v. 43, p. 867–870.
Rogers, J., 1996, Geology and tectonic setting of the Tawallah Group, southern McArthur Basin, Northern Territory: Doctoral dissertation, Hobart, University of Tasmania, 220 p.
Rohrlach, B.D., Fu, M., and Clarke, J.D.A., 1998, Geological setting, paragenesis and fluid history of the Walford Creek Zn-Pb-Cu-Ag prospect, Mt. Isa Basin, Australia: Australian Journal of Earth Sciences, v. 45, p.63–81.
Rox Resources, 2013, ASX Press Release, 18 September, 2013, 8 p.
——2016, ASX Press Release, 1 June, 2016, 21 p. (JORC Mineral Resource estimate completed by independent international consultants, AMEC Foster Wheeler).
Scott, D.L., Rawlings, D.J., Page, R.W., Tarlowski, C.Z., Idnurm, M., Jackson, M.J., and Southgate, P.N., 2000, Basement framework and geodynamic evolution of the Palaeoproterozoic superbasins of north-central Australia: An integrated review of geochemical, geochronological and geophysical data: Australian Journal of Earth Sciences, v. 47, p. 341–380.
Southgate, P.N., Bradshaw, B.E., Domagala, J., Jackson, M.., Idnurm, M., Krassay, A., Page, R.W., Sami, T.T., Scott, D.L., Lindsay, J.F., McConachie, B.M., and Tarlowski, C.Z., 2000, Chronostratigraphic framework for Palaeoproterozoic rocks (1730–1575 Ma) in northern Australia and their implications for base-metal mineralization: Australian Journal of Earth Sciences, v. 47, p. 461–483.
Taylor, M.I., McMillan, N.E, Dalrymple, I.J., and Hayward, N., 2017, Teena zinc-lead deposit, *in* Phillips, N., ed., Monograph 32 - Australian Ore Deposits: Australian Institute Mining and Metallurgy Bulletin, p. 483.
Williams, N., 1978, Studies of the base metal sulfide deposits at McArthur River, Northern Territory, Australia: II. The sulfide-S and organic-C relationships of the concordant deposits and their significance: Economic Geology, v. 73, p.1036–1056.

**Nick Hayward** is the Director of Global Project Generation, Exploration with Teck Resources, principally focused on driving large copper, zinc, and gold discoveries. Previously, he held roles with Teck Exploration as their Global Zinc Specialist and Chief Geoscientist for Asia-Pacific and Africa, following 5 years with BHP Billiton as Global Practice Leader (Structural Geology and Resource Targeting), and 20 years with WMC Resources. Nick has extensive technical leadership, global project generation, and project management experience for base metals and bulk commodities. He completed his Ph.D. in Structural Geology and Tectonics at James Cook University of North Queensland in 1991.